ELSEVIER

Journal of Structural Geology 29 (2007) 2017–2037

JOURNAL OF STRUCTURAL GEOLOGY

www.elsevier.com/locate/jsg

Deformation features within an active normal fault zone in carbonate rocks: The Gubbio fault (Central Apennines, Italy)

Maura Bussolotto [a,*], Antonio Benedicto [a], Chiara Invernizzi [b], Luca Micarelli [c], Valérie Plagnes [d], Giovanni Deiana [b]

[a] *Université Paris Sud XI, Laboratoire de Tectonique, CNRS/INSU, UMR 7072, 91405 Orsay, France*
[b] *Dip. Scienze della Terra, Università di Camerino, Italy*
[c] *Beicip-Franclab, 232, Av. Napoléon Bonaparte, BP 213, 92502 Rueil-Malmaison, France*
[d] *UMR Sisyphe, Université Pierre et Marie Curie, Paris VI, 75005 Paris, France*

Received 15 November 2006; received in revised form 16 July 2007; accepted 23 July 2007
Available online 6 August 2007

Abstract

The Gubbio fault is an active normal fault defined by an important morphological scarp and normal fault focal mechanism solutions. This fault truncates the inherited Miocene Gubbio anticline and juxtaposes Mesozoic limestones in the footwall against Quaternary lacustrine deposits in the hanging wall. The offset is more than 2000 m of geological throw accumulated during a poly-phased history, as suggested by previous works, and has generated a complex zone of carbonate-rich fault-related structures. We report the results of a multidisciplinary study that integrates detailed outcrop and petrographic analysis of two well-exposed areas along the Gubbio fault zone, geochemical analysis (fluid inclusions, stable isotopes, and trace elements) of calcite-sealed fault-related structures and fault rocks, and biostratigraphic controls. Our aims are: (i) the characterization of the deformation features and their spatial–temporal relationships, and (ii) the determination of the *P*/*T* conditions and the fluid behaviour during deformation to achieve a better understanding of fluid–rock interaction in fault zones.

We show that few of the observed structures can be attributed to an inherited shortening phase while the most abundant structures and fault rocks are related to extensional tectonics. The outcropping extensional patterns formed at depths less than 2.5–3 km, in a confined fluid system isolated from meteoric water, and the fault structures are the response to a small amount of cumulated displacement, 12–19% of the total geological throw.

Keywords: Fault rocks; Carbonates; Deformation mechanisms; Stable isotopes; Fluid inclusions; Displacement; Fluid–rock interaction

1. Introduction

The development of fault zone deformation features in carbonate rocks is related to *P*/*T* conditions, lithology, and fault displacement and conditioned by the presence of circulating fluids (Micarelli et al., 2005, 2006 and references therein). In recent years, research, coupling different methodologies, has revealed the role of these factors in fault-related deformation.

Recent works that combine microstructural analysis with paleothermometric analysis allow the characterization of the *P*/*T* (depth) behaviour during faulting (Micarelli et al., 2005; Benedicto et al., in press). Other works have focused on fault- and fracture-related calcites coupling microstructural, petrologic, and geochemical analyses; these works permit identification of different generations of calcite and investigations of fluid sources, flow pathways and fluid-driven mass transfer through faults (e.g. Travé et al., 1998; Boles and Grivetti, 2000; Sibson, 2000; Cello et al., 2001; Pili et al., 2002; Labaume et al., 2004; Benedicto et al., in press).

Our study integrates field macro and mesostructural analyses, microstructural analyses of thin sections by using classical, optical and cathodoluminescence microscopy, and paleothermometric analyses from fluid inclusions coupled with

* Corresponding author. Fax: +33(0)1 69 15 49 05.
E-mail address: maura.bussolotto@libero.it (M. Bussolotto).

0191-8141/$ - see front matter © 2007 Elsevier Ltd. All rights reserved.
doi:10.1016/j.jsg.2007.07.014

geochemical analyses (stable isotopes and trace elements) of syn-kinematic fault-related calcites. Furthermore, in the studied outcrops, we have performed some biostratigraphic controls that have been used as a tool to constrain fault displacement.

Here, we describe the deformation features and investigate their spatial organisation and their relative chronology. The influence of *P*/*T* conditions, lithology and fault displacement on the deformation mechanisms and related structures and fault rocks is also investigated in order to better constraint the evolution of the active Gubbio normal fault. Furthermore, geochemical analyses (stable isotopes and trace elements) of fault-related calcites provide a better understanding of fluid provenance and fluid–rock interaction within the fault zone.

2. Geological setting

The North-central Apennines chain is a NE-verging fold-and-thrust belt that resulted from the convergence between the Sardo-Corso block (European plate) to the west and the Adriatic block (African plate) to the east, since the Cretaceous (Dewey et al., 1989). The accretion process through the Adriatic continental margin (lower Oligocene–Pleistocene) has been accompanied by Tyrrhenian back-arc extension (Kastens et al., 1988) since the Miocene. The North-central Apennines presents two well-differentiated, adjacent domains (Fig. 1c; Alfano et al., 1982; Barchi et al., 1998). The Adriatic domain to the east (Fig. 1c) preserves compressional structures with Upper Miocene–Quaternary thrusting and related foredeep and/or piggyback basins (Collettini et al., 2000; Pauselli and Federico, 2003). To the west, the Tyrrhenian domain contains the inherited shortening structures of the chain overprinted by middle Miocene-to-Recent extensional deformation (Calamita and Pizzi, 1994; Cello et al., 1997). The extensional process has led to the formation of NW–SE trending normal faults and oblique-to-orthogonal strike-slip faults. Extensional features are progressively younger to the east and they controlled the development of Pliocene-to-Quaternary intramontane basins (Fig. 1). Normal and strike-slip faulting in the Tyrrhenian domain are coeval with active compression in the Adriatic domain (Elter et al., 1975).

The Umbria sector, where the Gubbio structure is located, can be considered as the transition between these Adriatic and Tyrrhenian domains (Boschi et al., 1997; Barchi et al., 2000; Collettini et al., 2003) and is characterized by NNW–SSE trending, SW dipping active normal faults (e.g. the Norcia earthquake, 1979, Ms = 5.9; the Gubbio earthquake, 1984, Ms = 5.2; the Colfiorito earthquake, 1997, $M_{max} = 5.9$; Boschi et al., 1997; Cello et al., 1997; Boncio and Lavecchia, 2000). These features overprint the thrust edifice built up since the late Miocene and involve the sedimentary succession (Umbria–Marche succession; Fig. 1b) and the underlying basement. The sedimentary succession is from bottom to top: evaporitic rocks (*Anidriti di Burano Fm*, Upper Triassic; about 1500 m thick); carbonate multilayers composed of Upper Triassic to Lower Liassic carbonate neritic sequence of massive limestones (*Calcare Massiccio Fm*; about 700–800 m thick), Middle Lias to Miocene well-bedded calcareous and calcareous-marly–cherty pelagic and hemipelagic sequence (900–1400 m thick); and siliciclastic turbiditic syn-orogenic deposits (*Marnoso-Arenacea Fm*, up to 4000 m thick) of lower Miocene–Pleistocene age that are progressively younger from the west to the east (Deiana and Pialli, 1994).

In this sector, seismic profiles show the presence of a regional east-dipping, low-angle normal fault, the Alto Tiberina fault (Fig. 1), which is interpreted as the basal detachment onto which outcropping normal faults, i.e. the Gubbio fault, connect with a listric geometry (Boncio et al., 1998, 2000; Barchi et al., 1999; Collettini et al., 2000; Boncio and Lavecchia, 2000). Modern seismicity is localized between the Alto Tiberina fault and the antithetic Gubbio fault (Boncio et al., 1998).

The Gubbio structure is one of the typical kilometre-scale folds cropping out in the external zone of the North-central Apennines (Figs. 1 and 2), where the Mesozoic–Paleogene sedimentary succession crops out between the terrigenous Miocene successions. The Gubbio fold axial plane strikes N135° and the fold's western limb is cut by a normal fault (Fig. 2), which strikes N110–N130° and juxtaposes the folded Mesozoic marine limestones in the footwall against the Plio-Quaternary lacustrine deposits in the hanging wall (Menichetti and Minelli, 1991; Boncio and Lavecchia, 2000).

Recently, the Gubbio fault has been the subject of numerous studies focused on seismic activity (Boncio and Lavecchia, 2000; Collettini and Barchi, 2002), fault geometry at depth and relations with inherited thrusting and folding (Menichetti and Minelli, 1991; Collettini et al., 2003; Mirabella et al., 2004), related basin geometry, and morpho-tectonic and sedimentary patterns (Collettini et al., 2000). Mirabella et al. (2004) describe the Gubbio fault as a multi-phase major fault with more than 2000 m of cumulative displacement that accommodated a geological throw of 850 m during the Lower Miocene extension and 1350 m during the Quaternary extension. They also suggest that during Upper Miocene NW–SE compression, the deeper part of the Gubbio fault was reactivated as reverse fault generating the Gubbio anticline.

3. Methods

Fault-related features such as slip planes, calcite-sealed veins, calcite-cemented breccias, and/or cataclasites (see below) are described in the field at outcrop scale (Figs. 3 and 4). Microstructural characteristics and cross-cutting relationships were defined by analyzing about 50 thin sections, using polarizing and cathodoluminescence microscopy. For cathodoluminescence analysis we used a Cold Cathodoluminescence Model (Technosyn 8200 M411) at 12–16 kV and 450–550 μ gun current and 0.05 Torr vacuum.[1]

After a preliminary petrographic examination of 21 double polished sections for fluid inclusion analyses, 12 samples were selected for fluid inclusion microthermometric analysis. This was performed by a U.S.G.S. heating–freezing stage.[2] The thermocouple was calibrated using synthetic standards with pure water (0 and 374.1 °C) and pure CO_2 (−56.6 °C). Sample

[1] UMR-IDESS of the University of Paris Sud XI, Orsay (France).
[2] Fluid inclusion laboratory of University of Camerino, Camerino (Italy).

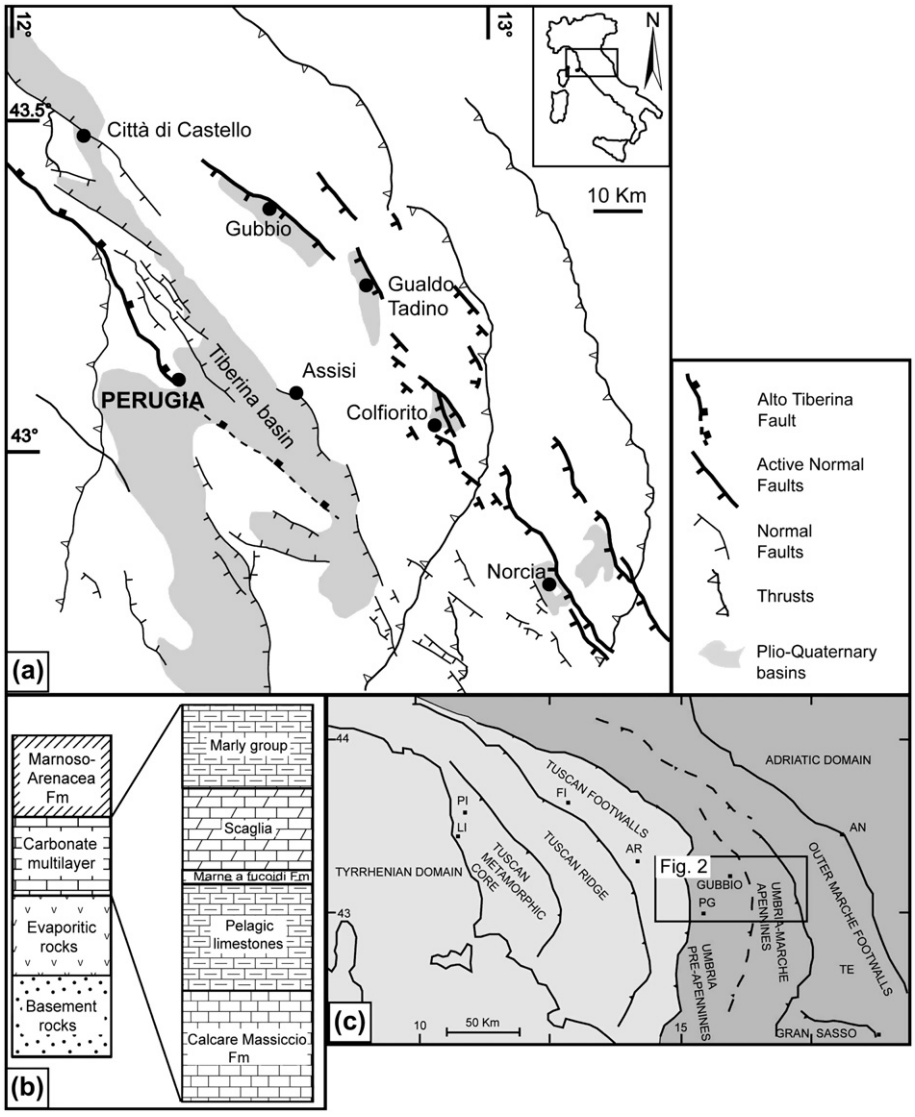

Fig. 1. (a) Schematic geological map of Central Apennines (after Pauselli and Federico, 2003); (b) schematic Umbria–Marche stratigraphic succession (see text for details); (c) sketch of Northern Apennines. Light grey: Tyrrhenian domain; dark grey: Adriatic domain (from Pauselli and Federico, 2003).

preparation and measurement procedure are well described in Goldstein and Reynolds (1994) and Munchez et al. (1994). To avoid the risk of re-equilibration due to ice growth in inclusion cavities contained in soft minerals, we first measured the homogenization temperatures (T_h), to have indication on entrapment *P/T* conditions (Goldstein and Reynolds, 1994), and secondly the final ice melting temperatures ($T_{m\text{-}ice}$), to obtain fluid salinity (Bodnar, 1993). The T_h was reproducible to within 1 °C and $T_{m\text{-}ice}$ to within 0.1 °C.

Samples of the carbonate host rock and calcite cements in veins and breccias were analyzed by a VG Sira mass spectrometer[1] in order to determine their isotopic composition (^{13}C and ^{18}O). Samples were mechanically drilled from polished surfaces. Powdered sample was reacted with 2 ml of orthophosphoric acid at 25 °C under vacuum (following Craig, 1957). Isotope results are expressed as per mil (‰) deviation (δ) from the VPDB (Vienna Pee Dee Belemnite) standard. Reproducibility of both carbon and oxygen measurement is 0.1‰.

Determination of trace elements in calcite cements was performed by inductively coupled plasma atomic emission spectrometry (ICP-AES). Powdered samples (15 mg) were reacted with 2 M nitric acid (10%) and water to form a total volume of 10 ml. This plasma was analyzed by Isa Jobin Yvon JY 24, Division d'instruments Sa[3] to calculate ppm concentrations of Fe, Mn, Si, Mg, and Sr.

In order to evaluate fault displacement within the fault zone some micropaleontological controls[4] on samples of limestones involved in the studied fault zone were carried out. Our considerations about fault geological throw are based on the Bottaccione stratigraphic section (Premoli Silva and Sliter, 1994). All analyzed samples are shown in Table 1.[2]

[3] CIGA laboratory of University of Camerino (Italy), Dr Laura Petetta.

[4] Biostratigraphy laboratory of University of Camerino, Camerino (Italy), Dr Petros Didaskalou.

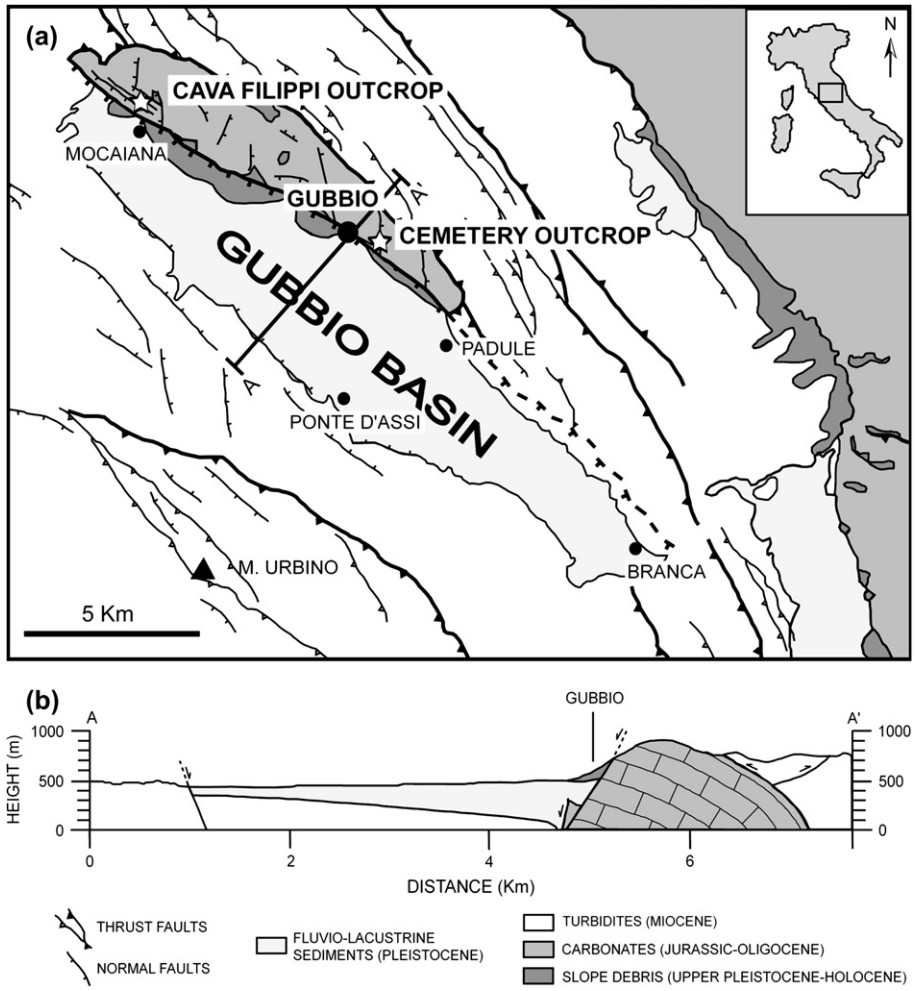

Fig. 2. (a) Simplified map of the Gubbio area and (b) geological cross-section of the Gubbio structure modified after Menichetti and Minelli, 1991; Collettini et al., 2000, 2003 and Mirabella et al., 2004. White stars locate analyzed outcrops.

4. Fault zone analysis

We studied two exposures across the Gubbio fault, both situated within the fault footwall. The Cava Filippi outcrop is located near the NW fault termination (Fig. 2) in a quarry high on the fault scarp. The outcrop exhibits a high quality, fresh section about 50 m thick and orthogonal to the fault trace (Fig. 3). The second section, called the Cemetery outcrop, is located along the central part of the fault along a secondary road that passes the Gubbio town cemetery (Fig. 4).

The Cava Filippi outcrop exposes a 50 m thick fault zone between the undeformed limestones of the footwall and the main fault escarpment which bounds the Plio-Quaternary basin-fill deposits (Fig. 3). The fault zone deforms grey/white platy limestones of the lower (calcareous-selcifer member) and the middle (reddish marly-calcareous) members of *Scaglia rossa Fm* (Coniacian–Upper Palaeocene). Limestone layers are10–20 cm in thickness.

Six well-defined structural domains can be depicted (Df-0 to Df-5 in Fig. 3), separated by five major, SW dipping normal slip planes (Ff-1 to Ff-5 in Fig. 3). Stratification gently dips basinward in the inner (Df-0) domain (N100–15°SW) and is moderate to highly tilted external domains (N127–50°SW).

Domain Df-0 corresponds to the undeformed footwall. Around 1.5 m northeast of Ff-1 domain, bedding is gently dragged downward. Some low-angle, flat-ramp shaped slip planes (striking N110°; Fig. 3b), locally marked by calcite mineralization, are present. In places, incipient layer brecciation is associated with the flat slip planes. Calcite-sealed fractures, homogenously distributed in this domain, are also present; they are sub-vertical and orthogonal to bedding (striking N100–N120°; dipping 70°NE–90°) or conjugate strike-slip fractures (striking N–S and N050–N070°). The Df-0 outer boundary is a normal fault (Ff-1) laced with a lens of breccia (Fig. 3b). The Ff-1 fault plane is characterized by random fabric cataclasite (some tens of centimetres thick) located in both the footwall and the hanging wall (Fig. 3b).

Domain Df-1 is characterized by highly fractured, but well recognizable, tilted bedding. Limestone layers are tilted. Sets of open-extensional/shear fractures (striking N130–N155°) are present. They are oblique to bedding and bounded by bedding planes. Where shear is present, displacements up to 2 cm

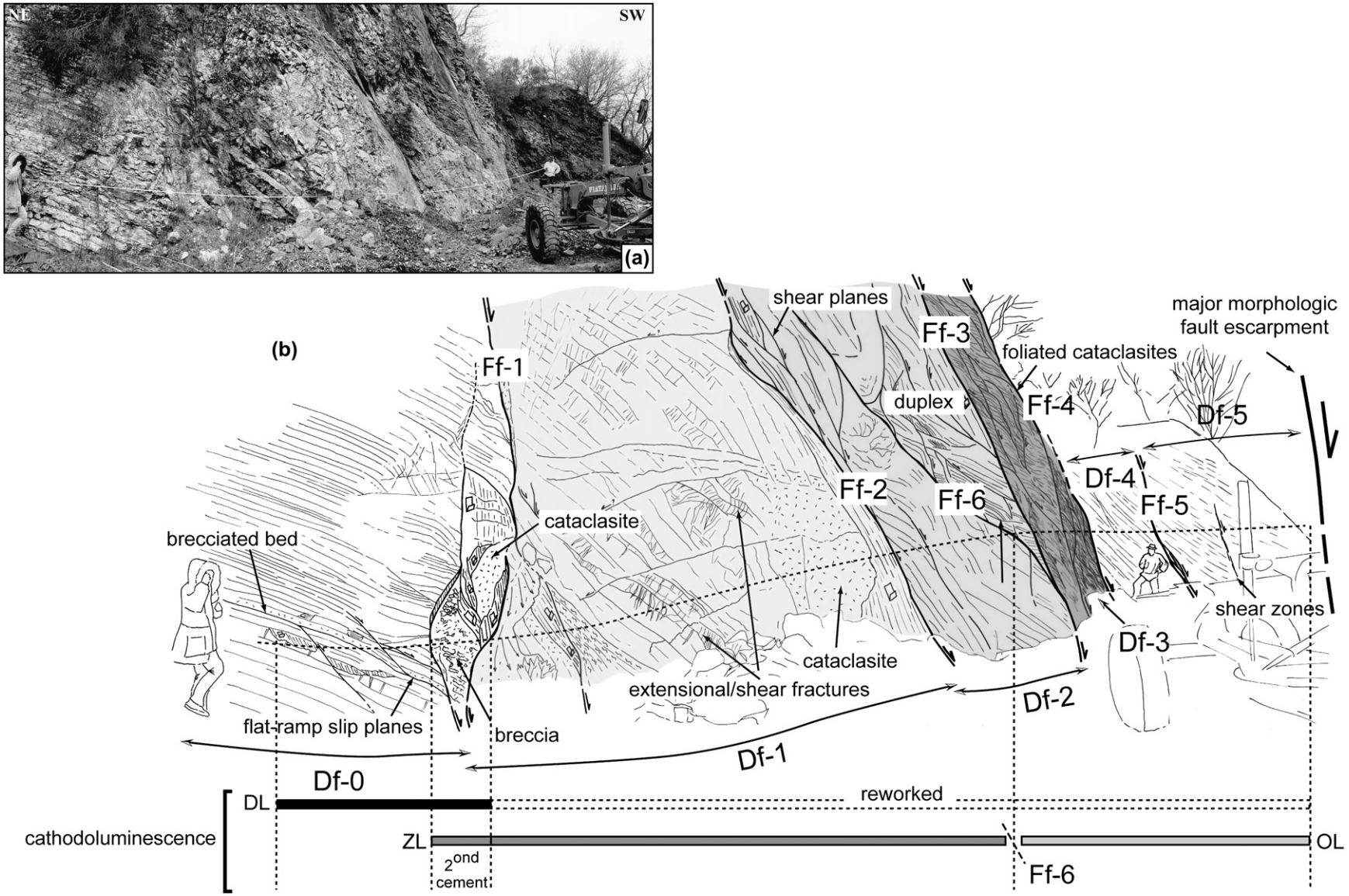

Fig. 3. (a) The Cava Filippi outcrop and (b) line-drawing outlining the main structural patterns and the spatial distribution of fault-related calcite types shown by cathodoluminescence analyses.

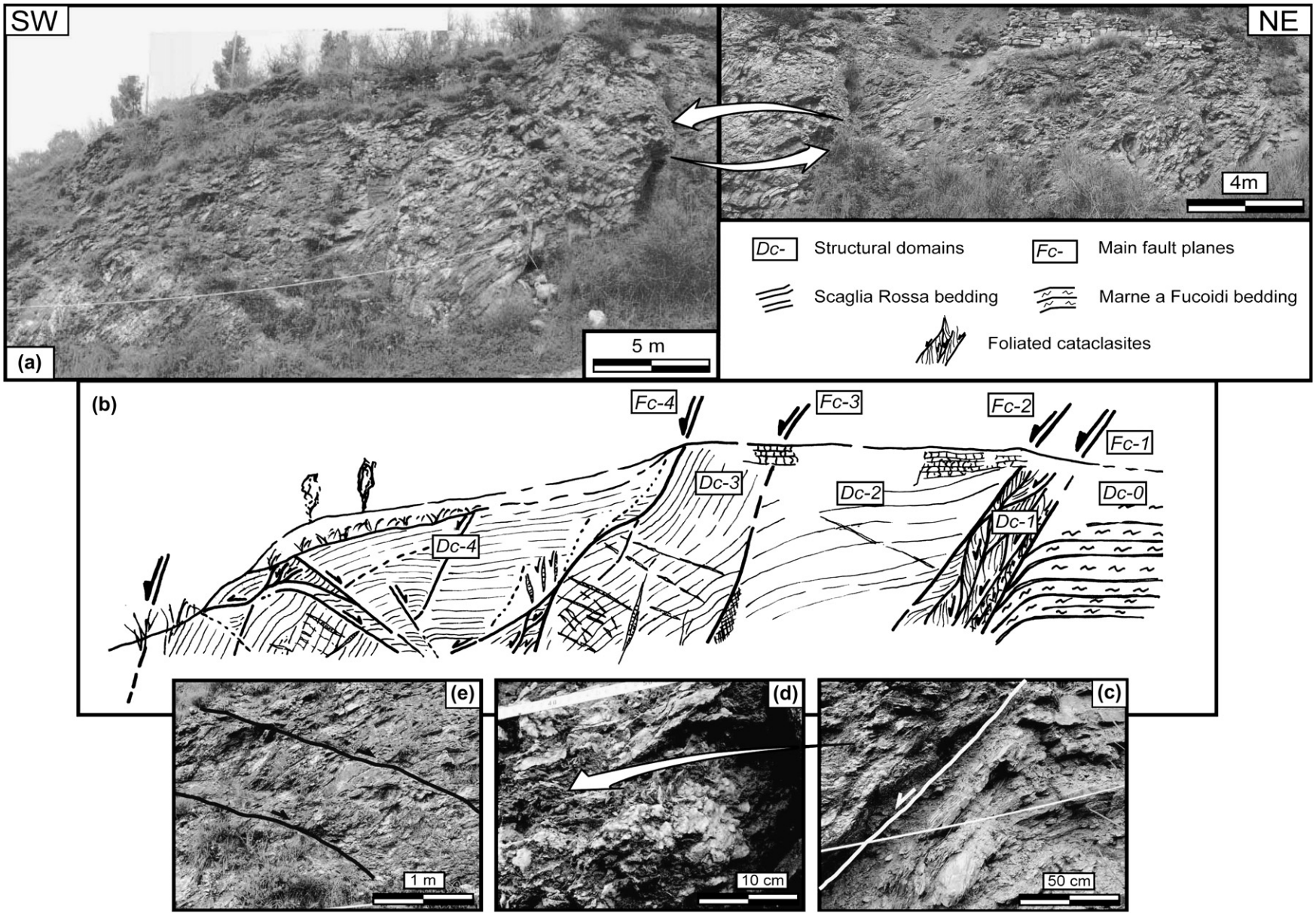

Fig. 4. (a) The Cemetery outcrop; (b) simplified sketch showing the main structural domains separated by major SW dipping, fault planes. Cemetery outcrop details; (c) Dc-0 (footwall) highly sheared clayey layer dragged in Fc-1 fault plane; (d) details of foliated cataclasites in Dc-1 domain; (e) low-angle antithetic fault planes in Dc-4 domain.

Table 1
Compiled data for the analyzed samples

Cava Filippi samples	Calcite types	Microthermometry analyses	Isotopes analyses	ICP-AES analyses	Stratigraphic controls
G-1	DL				
G-2	DL	×	×		
G-3	DL			×	
G-4	DL				
G-5	DL	×	×		
G-6	DL	×			
G-7	DL				
G-8	DL				
G-9	ZL + DL		×		
G-10	ZL + DL	×			
G-11	ZL + DL				
G-12	ZL	×			
G-13	ZL	×	×	×	
G-14	ZL				
G-15	ZL + DL		×		
G-16	ZL + DL	×	×		
G-17	ZL + DL				
G-18	ZL + DL				
G-19	ZL + DL		×		
G-20	OL	×	×		
G-21	OL				
G-22	OL				
G-23	OL + DL	×			
G-24	OL + DL				
G-25	OL + DL				
G-26	OL + DL	× ($T_{m\text{-}ice}$)			
G-27	OL + DL				
G-28	OL + DL	×			
G-29	OL + DL	×	×	×	
G-30	OL + DL	× ($T_{m\text{-}ice}$)			
G-31	OL + DL		×		
G-32	OL + DL				
G-33	OL + DL	×	×		
GS1					×
GS3					×
GS5	DL	×			
GS7					×
GS8					×
GS9					×
GS10					×
GS11					×
GS12					×

Cemetery samples	Calcite types	Microthermometry analyses	Isotopes analyses	ICP-AES analyses	Stratigraphic controls
Gc-1	DL				
Gc-2	DL				
Gc-3	DL	×	×	×	
Gc-4	DL				×
Gc-5	OL				×
Gc-6	OL				×
Gc-7	OL				×
Gc-8	ZL + DL	×	×		×
Gc-9	OL				×
Gc-10	OL	×	×		×
Gc-11	OL				×
Gc-12	OL	×	×	×	
Gc-13	ZL	×	×	×	×
Gc-14	OL	×			
Host rock (Cava Filippi outcrop)					
G-2-C			×		
G-20-C			×		
G-33-C			×		
Host rock (Cemetery outcrop)					
Gc-8-C			×		
Gc-10-C			×		
Gc-11-C			×		
Gc-13-C			×		

are recognized. They are mostly partially filled by drusy calcite and, in places, by yellow/red clays. Calcite veins orthogonal to bedding and conjugate strike-slip fractures observed in the Df-0 are also present here.

Furthermore, domains Df-0 and Df-1 are characterized by very abundant solution seams with stylolite teeth up to half a centimetre in size. Most of the stylolites are parallel or subparallel to bedding. These well-developed stylolites are not observed in the footwall (Df-0). They seem neo-formed during faulting or reactivated and overdeveloped under extensional strain if they previously formed related to rock compaction. Solution seams accommodate deformation of dragged layers and bed thinning when approaching fault slip planes Ff-2 and Ff-3.

Domain Df-2 is characterized by shear planes and extensional duplex structures which are easily identifiable because of the well-preserved bedding planes (Fig. 3); these structures are localized in red limestones richer in marls. In the Df-2 domain, open-extensional/shear fractures, partially filled by drusy calcite, are still present: here, observed shear displacements up to 2 cm are common.

Domain Df-3 is characterized by 2 m thick zone of foliated carbonate cataclasite (foliation N127–83°SW; minor shear planes: N140–53°SW) which obliterates bedding (Fig. 3b). Lithons are almost constituted by kinematic calcite and bounded by thin, red/brown marly rims.

The last two domains (Df-4 and Df-5) are developed in marly red limestones. Bedding, about 5 cm thick, is strongly tilted basinward (N130–48°SW) and cross-cut by moderate dipping shear zones underlined by calcite lenses and centimetre-scale pull-apart structures. Some veins orthogonal to bedding affect limestone layers. The Df-4 and Df-5 domains are separated by a major fault plane (Ff-5) characterized by strongly dragged and thinned marly layers that suggest a significant offset.

The Cemetery exposure preserves a 50 m thick fault zone less rich in structures than the Cava Filippi outcrop (Fig. 4). The stratigraphic sequence here is slightly older as the lowest footwall fault plane (Fc-1) juxtaposes the grey marls and the marly limestones of the *Marne a Fucoidi Fm*, constituting the undeformed footwall, against the marly limestones of the *Scaglia rossa Fm* which are involved within the fault zones and separated from the Plio-Quaternary basin-fill deposits by a major morphological escarpment.

The outcropping fault zone can be characterized by five structural domains. The Dc-0 structural domain corresponds to the footwall, while the Dc-1 to Dc-4 domains are involved within the fault zone. Structural domains are separated by five major fault planes (Fc-1 to Fc-5 in Fig. 4b).

In the footwall (Dc-0), marly limestone layers are 3–5 cm thick, horizontal or very gently tilted toward the basin (N122–08°SW). Bedding is strongly dragged close to the first fault plane (Fc-1; Fig. 4c) and is characterized by flexural extensional fractures associated with normal faulting. Sub-vertical, conjugate strike-slip fractures and veins orthogonal to bedding are also present.

Fault Fc-1 is defined by a 10 cm thick, highly sheared clayey gouge, dragged or smeared in the sense of Weber et al. (1978), Harding and Tuminas (1989) and Lindsay et al. (1993) within the fault (Fig. 4c).

Domain Dc-1 is dominated by a 5 m thick foliated, marly cataclasite (Fig. 4d). It consists of highly sheared calcite lithons with a marly matrix with, in places, S–C fabrics (shear planes: N160–40°SW) that support a normal fault offset.

In domain Dc-2, bedding is gently tilted toward the basin and easily recognized. Some calcite-filled fractures orthogonal to bedding and bed-confined are remarkable.

Domain Dc-3 is characterized by highly tilted bedding (N135–40°SW) and a dense network of calcite-filled open-extensional/shear fractures, mostly bed-confined, striking N110–120°. In places calcite is of the drusy type. Also extensional fractures, orthogonal to bedding, and ramp/flat slip planes, marked by calcite mineralization, are locally present.

Fc-3 and Fc-4 normal faults are associated with thin zones of random cataclasite.

Domain Dc-4 displays mainly synthetic and antithetic secondary normal faults (N120–35°NE, Fig. 4e) with abundant calcite mineralization. Partially calcite-sealed open-extensional/shear fractures are present. Solution seams sub-parallel to the stratification are remarkable through the whole outcrop. Calcite open-extensional/shear fractures are frequently offset by these solution seams.

4.1. Microstructural and petrological analysis of common mesostructures

Mesostructural description of both the outcrops allows us to recognize 10 different types of common deformation patterns: strike-slip fractures, extensional fractures orthogonal to bedding, open-extensional/shear fractures, solution seams (stylolites), secondary synthetic or antithetic low-angle slip planes, major fault planes, fault rocks (breccias, random fabric cataclasites, and foliated cataclasites), and shear zones.

In this section, we describe the microstructural and petrologic characteristics of those common deformation patterns, and establish their relative chronology with cross-cutting relationships. Special attention is later focused on calcite-filled fault-related structures.

Strike-slip fractures (Fig. 5a) are organized into conjugate systems striking N–S (sinistral) and N50–N70° (dextral) compatible with a NE–SW oriented extension (De Paola et al., 2006) and a NW–SE compression. They are calcite-sealed, generally from 2 to 5 mm thick, and show calcite striae parallel to bedding.

Extensional fractures orthogonal to bedding (Fig. 5c) are stratabound, calcite-sealed veins up to 2–3 cm thick. They strike N100–N120° (i.e. parallel to the Gubbio fault trace). Both strike-slip fractures and fractures orthogonal to bedding are filled by large, anhedral, sometimes elongated calcite crystals (Fig. 5b, d). Crystal dimension (<1–2 mm) increases toward the center of the veins. Calcite crystals are characterized by dense, thin mechanical twins, and strong undulose extinction. Crystal boundaries are regular and locally lobate. Both types of fractures are cross-cut by the open-extensional/shear

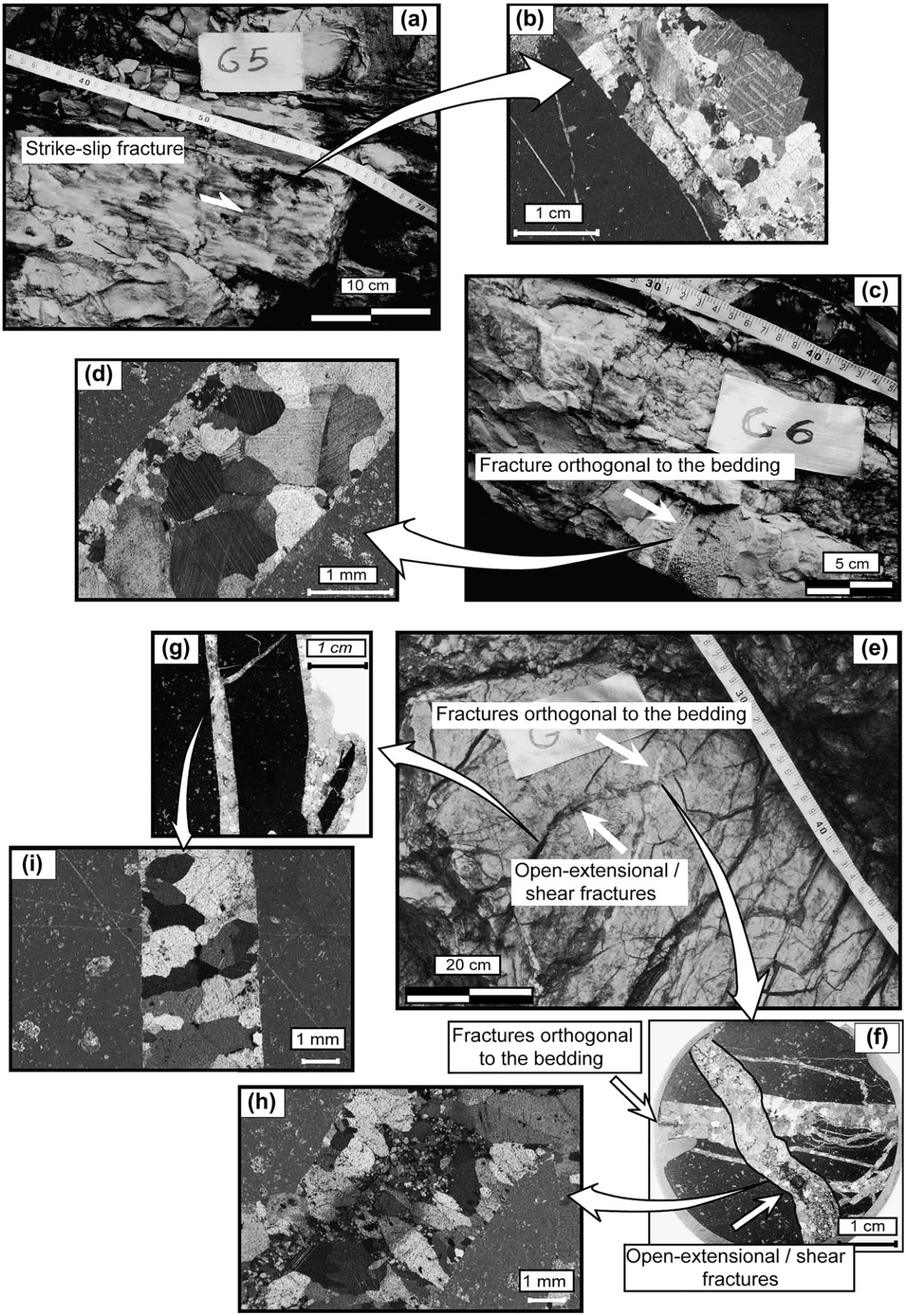

Fig. 5. (a) Strike-slip fractures; the white arrow indicates the sense of motion; (b) microscope detail of strike-slip fractures; (c) veins orthogonal to bedding; (d) microscope detail of fractures orthogonal to bedding; (e) open-extensional/shear fractures. Open-extensional/shear fractures cross-cut fractures orthogonal to bedding; (f) and (g) open-extensional/shear fractures in thin section. In figure fracture boundaries have been underlined; (h) and (i) microphotographs of open-extensional/shear fractures.

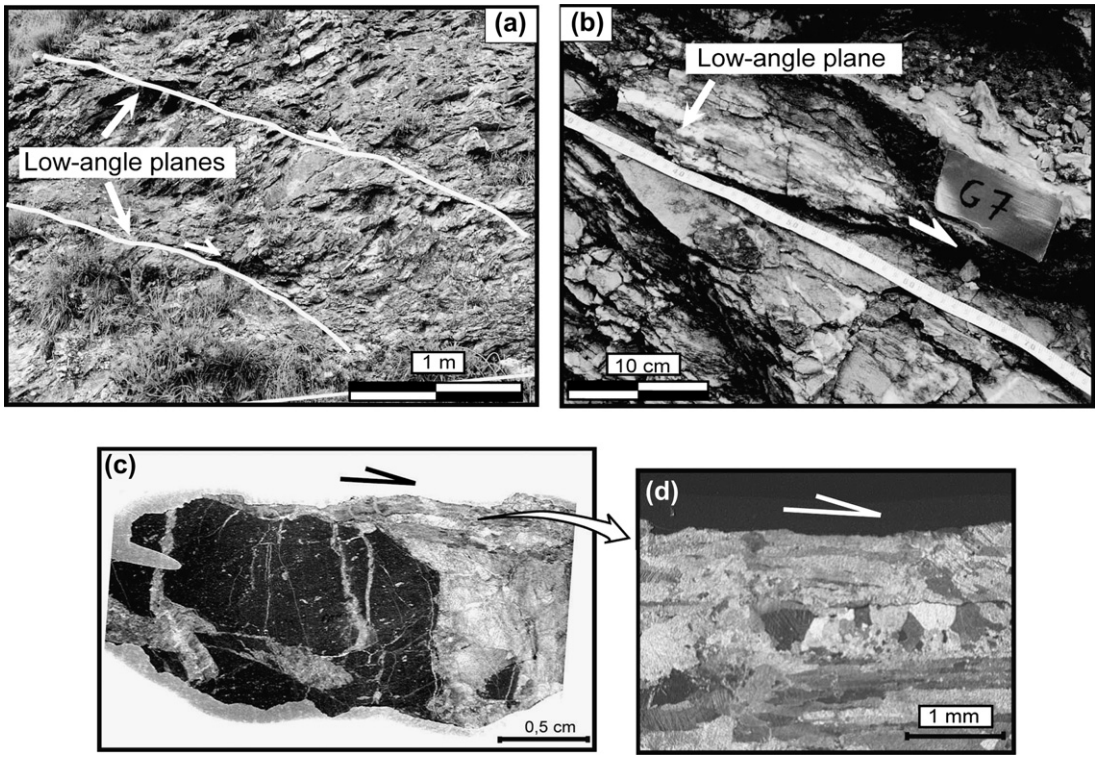

Fig. 6. Low-angle fault planes: (a) details of a synthetic plane in Cava Filippi outcrop; (b) antithetic plane in the Cemetery outcrop; (c) and (d) microscope details of calcite associated with this plane.

fractures or reworked in fault rocks indicating their relative older chronology.

Open-extensional/shear fractures (Fig. 5e) are parallel to the Gubbio fault trace. They are oblique to bedding, antithetic or synthetic to the Gubbio fault and are layer-restricted. They show pure extensional or shear displacement <2 cm of offset. These fractures are up to 3 cm thick and are partially filled by calcite and/or yellow/red clays. Calcite crystals are anhedral and locally contain thin mechanical twinned, or sub-hedral and twin-free. Crystal size increases toward the inner part of veins (up to 5–6 mm in size) where drusy calcite is often present (Fig. 5f–i). Crystal boundaries are very regular, only in places weakly serrated. All crystals are characterized by weak undulose extinction.

Solution seams (stylolites) in the fault zone are an important and pervasive deformation feature at all scales. At the outcrop scale they present well-developed stylolite teeth up to half a centimetre in size and are mostly parallel or sub-parallel to the stratification. At microscopic scale, they are frequent within random cataclasites where they involve individual grains, and/or form continuous, irregular surfaces of intense dissolution highlighted by argillaceous rims. Close to slip planes, solution seams form an angle of 30–90° with the fault planes. Solution seams also bound foliated cataclasite sigmoids.

Secondary synthetic or antithetic low-angle slip planes (Fig. 6a, b), N110° striking, have flat-ramp geometries and are marked by calcite mineralization in places. Calcite is striated and made up of 200 μm to 3–4 mm large crystals, locally fibrous, elongated parallel to slip vector (Fig. 6c). Crystals are characterized by intense thin twins and by strong undulose extinction. Their boundaries are very irregular and generally serrated. These slip planes offset strike-slip and orthogonal to bedding fractures.

Major fault planes (see Figs. 3 and 4), striking N140–75°SW, cross-cut all the structures. They are simple undulating and smooth surfaces. Planes are striated due to both mechanical striation and calcite fiber growth, indicating pure normal (dip-slip) displacement (pitch 90°). In the Cava Filippi outcrop, major slip planes are associated with thick random fabric cataclasites. In the Cemetery outcrop, except for the Fc-1 and Fc-2 fault planes, the other major slip planes are associated with infrequent cataclasites.

Three types of fault rock are recognized in the outcrops: breccias, random fabric cataclasites, and foliated cataclasites.

A breccia fault rock is associated to the Ff-1 fault plane in Cava Filippi outcrop, where it constitutes a lens of ~50 cm thick (Fig. 7a), and the Fc-4 fault in Cemetery outcrop, where it constitutes a lens of about 20 cm thick. These lenses are made by angular limestone fragments (1 mm–2 cm in size)

Fig. 7. (a) Hydraulic breccia from Cava Filippi outcrop; (b) and (c) hydraulic breccia viewed in thin section; (d) thin section of breccia showing pression-solution surfaces forming approximately with a 90° angle to the fault plane (the arrow indicates the shear motion); (e) random fabric cataclasite associated with the Cava Filippi outcrop Ff-2 fault; (f) detail on a cut sample; (g) random fabric cataclasite viewed in twin section; (h) foliated cataclasites in the Cava Filippi outcrop; (i) thin section of foliated cataclasite and (j) magnified view.

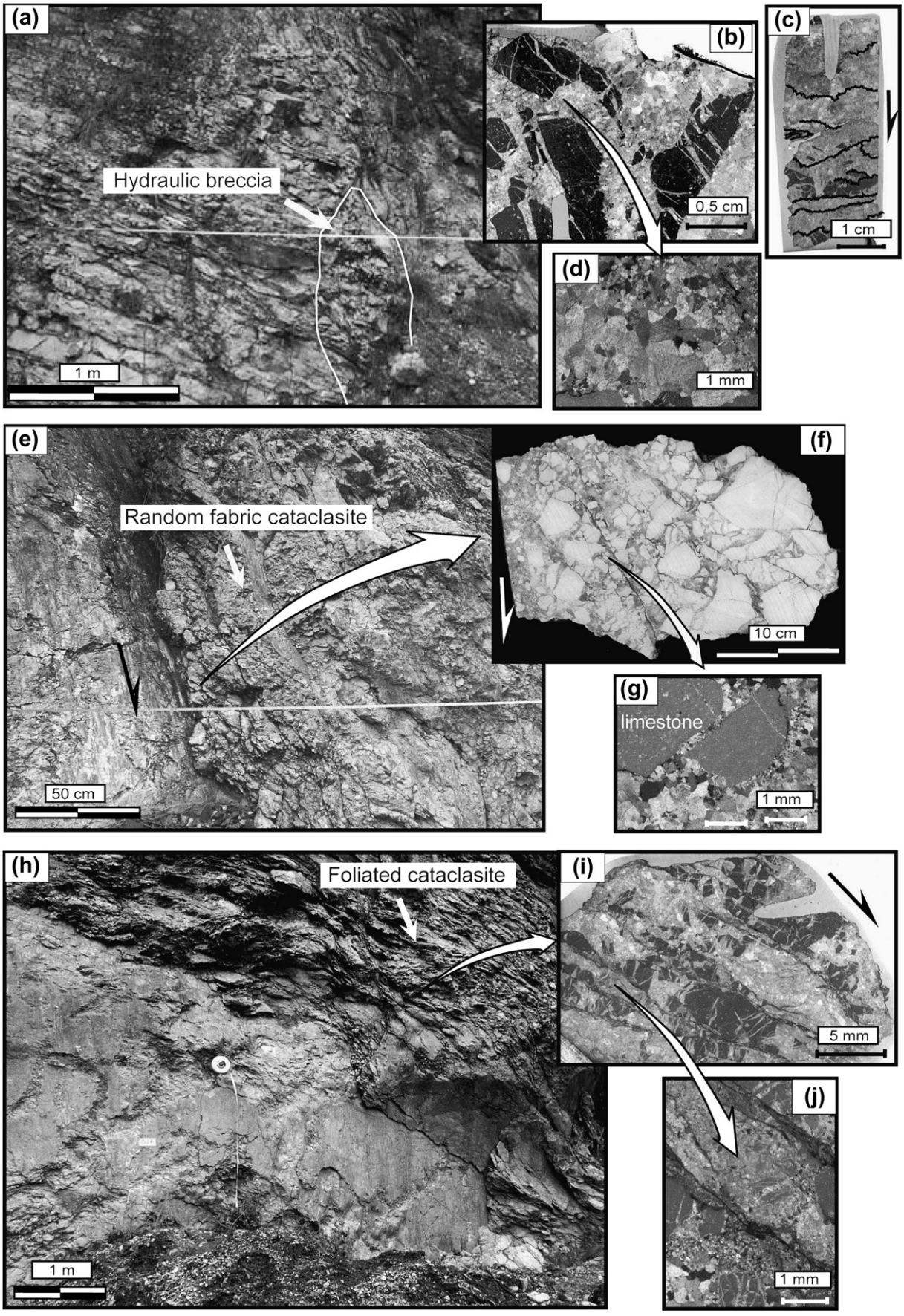
(a)
Hydraulic breccia
1 m
(b)
0,5 cm
(c)
1 cm
(d)
1 mm
(e)
Random fabric cataclasite
50 cm
(f)
10 cm
(g)
limestone
1 mm
(h)
Foliated cataclasite
1 m
(i)
5 mm
(j)
1 mm

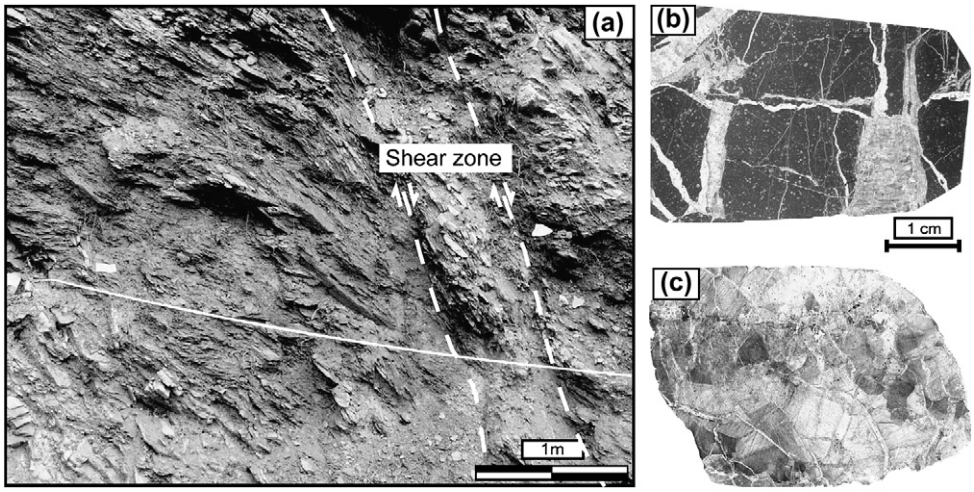

Fig. 8. (a) Example of a shear zone defined by centimetre sigmoidal shape lithons in the Cava Filippi outcrop; (b) thin section of a marly limestone lithon; (c) thin section of calcite bearing lithon.

that derive from adjacent host material and appear to have fragmented in situ due to bulk dilation. This texture suggests hydraulic brecciation as reported by Maltman (1998). They have not preferred alignment and they are sealed by calcite cement. Fragments commonly show very irregular boundaries (Fig. 7b). Calcite cement consists of anhedral, intensely twinned crystals of different sizes (from 500 μm up to 8 mm; Fig. 7d), characterized by undulose extinction. Locally, a second cement is recognizable. It has smaller (from 300 μm up to 600 μm; Fig. 7d) untwinned crystals, characterized by very irregular and serrated boundaries, and an orthogonal relationship to the vein walls. Moreover, close to the fault plane, these breccias are overprinted by pressure-solution surfaces, forming approximately a 90° angle with the fault plane (Fig. 7c). These surfaces display an irregular geometry.

The most representative random fabric cataclasite is that associated to the Ff-2 fault plane in Cava Filippi outcrop. It is characterized by a 40 cm thick well-cemented cataclasite (Fig. 7e) consisting of host rock clasts, sealed by calcite cement. This cataclasite displays an increasing degree of deformation toward the fault plane as well as decreasing fragment size (Fig. 7f). Calcite cement crystals are small in size (from 100 μm up to 200 μm; Fig. 7g) and display dense thin twins and strong undulose extinction. A dense system of 1–5 cm spaced solution seams and orthogonal calcite veins is present. Solution seams are highlighted by argillaceous rims. Also, in the Cemetery outcrop, some centimetres of random cataclasites characterize Fc-3 and Fc-4 fault planes.

Foliated cataclasites constitute the Df-3 domain in the Cava Filippi outcrop (Fig. 7h), and the Dc-1 domain in Cemetery outcrop; they are bounded on each side by two major fault planes. Bedding is completely obliterated by a sigmoid shape foliation and calcite lithons. At the outcrop scale, it is possible to distinguish a 20 cm thick layer, close to the Ff-2 fault, consisting of re-precipitated calcite and forming a well-organized S–C fabric (Fig. 7h, i). Foliation is defined by thin clay-rich rims, spaced from 500 μm up to 1–2 mm. A layer of small crystals with preferred orientation (about 200–300 μm in size; Fig. 7j) is related to the rims. Between adjacent rims it is possible to observe thinly twinned anhedral crystals of different sizes (from 200 μm up to 2 mm). Crystal boundaries are serrated and locally lobate; strong undulose extinction is observed. Outside this layer, the calcite percentage decreases and clay-rich rims are bedding-derived solution seams. Limestone sigmoids show old calcite veins perpendicular to solution seams and partially dissolved along the stylolites. In places these veins are re-opened and filled by elongated calcite crystals, about 2 mm in size, which show twinning and undulose extinction.

Shear zones, organized with S–C fabrics, involve the marly limestones (Df-4 and Df-5 domains in Cava Filippi outcrop; Fig. 8a). Shear zones strike parallel to major fault planes and are defined by marly limestones or sigmoidal, centimetre-scale calcite lithons bordered by clay rims. Marly limestone lithons are dissected by a network of calcite-filled fractures and solution seams (Fig. 8b). These fractures, <1 cm in thickness, show irregular boundaries and are filled by anhedral, large crystals (from 200 μm up to 4–5 mm in size). Crystals are in places elongated and their dimensions increase toward the center of the veins. When lithons are entirely formed by re-precipitated calcite, crystals are anhedral, from 3 mm up to 8–10 mm in size, and they show irregular boundaries (Fig. 8c). Calcite within shear zones is characterized by dense twins and undulose extinction.

5. Calcite cements analysis: paleothermometry and fluid origin

Cathodoluminescence analysis of calcite cements allows the identification of: a dull luminescent calcite (DL), a zoned luminescent calcite (ZL), and an orange luminescent calcite (OL).

DL-calcite (Fig. 9a, b) is dark reddish-brown coloured like the host rock. DL-calcite cements the hydraulic breccia in the Cava Filippi outcrop (Df-1), the strike-slip fractures, and the orthogonal to bedding extensional fractures of the Df-0 and

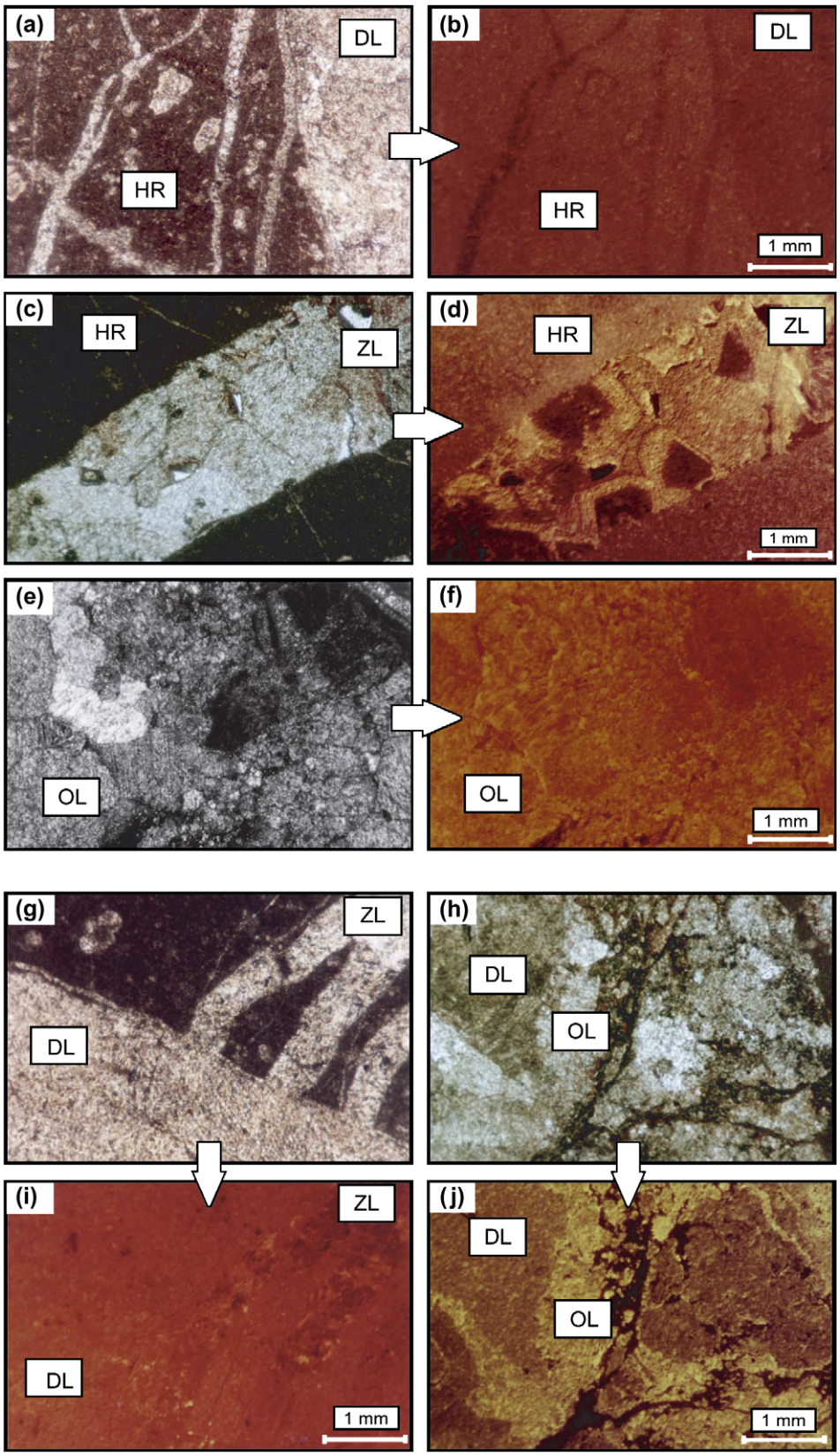

Fig. 9. DL-, ZL- and OL-calcite cements viewed under optic (a, c and e) and under cathodoluminescence microscope (b, d and f). Pictures from (g) to (j) show cross-cutting relationships between DL- and ZL-calcite (g and h) and OL-calcite (i and j).

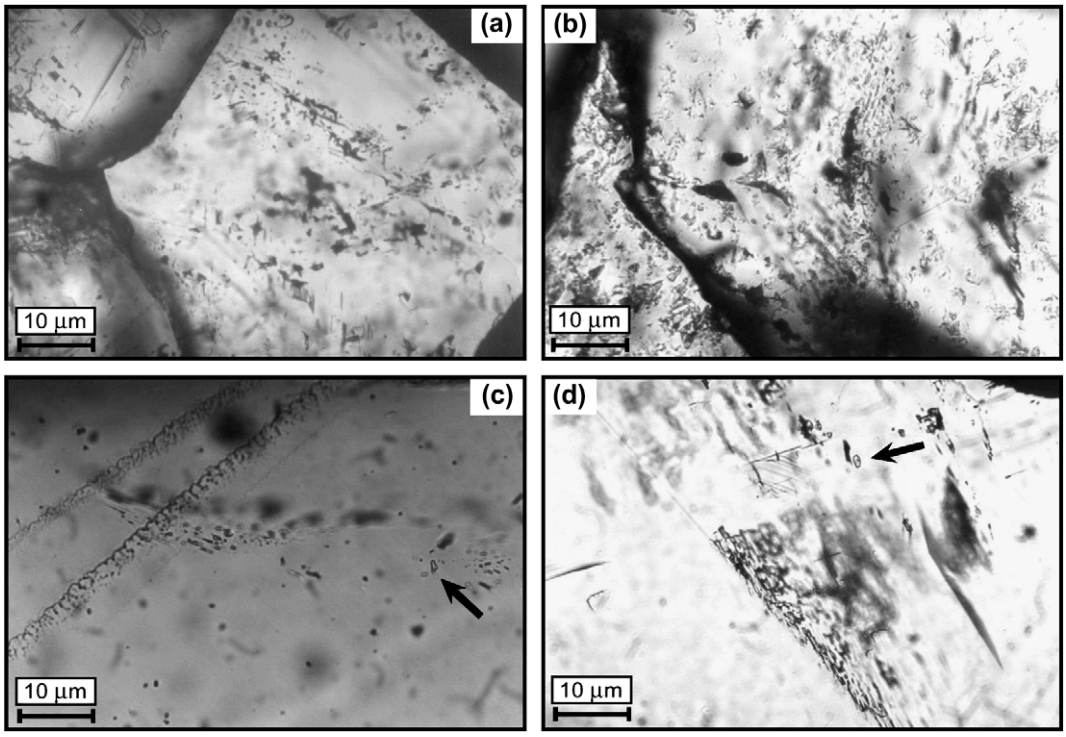

Fig. 10. Fluid inclusions: (a) example of decrepitated inclusions with dendritic shape in ZL-calcite (sample G-12); (b) example of decrepitated inclusions in OL-calcite (sample G-29); (c) and (d) black arrows indicates some small two-phase primary inclusions in DL-calcite (sample G-5).

Dc-0 domains. It is also characteristic of the secondary low-angle slip planes (i.e. Df-0, Dc-2, Dc-3, and occasionally in Dc-4). It has been also found as reworked fragments inside the cataclasites and the shear zones.

The ZL-calcite, zoned from brown to orange and yellow (Fig. 9c, d), fills the open-extensional/shear fractures in the Cava Filippi outcrop (but not those in the Cemetery outcrop), and the random cataclasites (Cava Filippi outcrop). Furthermore, it forms the second cement within the hydraulic breccia in the Cava Filippi outcrop and is the only cement of the hydraulic breccia in the Cemetery outcrop.

OL-calcite is orange luminescent (Fig. 9e, f). It fills up the open-extensional/shear fractures of the Cemetery outcrop, the foliated cataclasites of both outcrops, and the shear zones within the marly limestones in the Cava Filippi outcrop.

Cross-cutting relationships show that the DL-calcite is older than both ZL- and OL-calcite (Fig. 9g–j). Relationships between ZL-calcite and OL-calcite are not evident because they have different spatial distribution in the fault zone and they do not cross-cut each other.

In the Cava Filippi outcrop the spatial limit between ZL- and OL-calcite is represented by the Ff-6 fault that bounds the lower part of duplex structures in the Df-2 domain (Fig. 3). This boundary also coincides with the lithological change from grey/white limestones to red marly limestones.

Fluid inclusions analysis was performed by optical microscopy on 21 double polished wafers 150 µm thick (Table 1). Due to a large diffusion of mono-phase, leaked or decrepitated inclusions almost in all samples, and due to the very small inclusion size (often below the optical resolution for thermometric observations, Fig. 10), only eight samples were useful to collect microthermometric data from the Cava Filippi outcrop (4 in DL-, 2 in ZL-, and 2 in OL-calcite) and four samples from the Cemetery outcrop (1 in DL-, 2 in ZL-, and 1 in OL-calcite). In reference to the Cava Filippi outcrop, decrepitated inclusions with dendritic shapes are typical of an internal over-pressure development (Vityk and Bodnar, 1995) and they are most evident in calcite crystals from Df-0 to Df-2 domains. Most of Cemetery outcrop samples show a large percentage of mono-phase inclusions. Leakage, mainly related to fluid inclusion size (only inclusions larger than 15 µm have been leaked), is present in samples from all domains. In the Df-4, Df-5, Dc-3 and Dc-4 domains, mono-phase, irregular shape fluid inclusions and un-healed fluid inclusion planes are very common. Primary inclusions, oriented along the crystal growth direction or arranged in growth bands, are prevalent. Secondary inclusions, aligned along micro-fractures, are rare and too small to be analyzed. Therefore, most microthermometry data are collected from primary and pseudo-secondary well-preserved two-phase fluid inclusion assemblages with constant L/V ratio (vap% = 5–10). Data from Cava Filippi samples gave the following results: from DL-calcite (Fig. 11a), homogenization temperatures (T_h) have a mean value of 72 °C, and mean ice melting temperature ($T_{m\text{-}ice}$) is about −1 °C (Fig. 11b), corresponding to very low salinity water (1.74 wt% NaCl; Bodnar, 1993). Small, rounded, mono-phase inclusions observed in the same fluid inclusion assemblages are interpreted to be due to metastability and not due to necking down phenomena because bubbles re-appeared during the freezing or heating cycling. In ZL- and OL-calcite, large, irregular-shaped

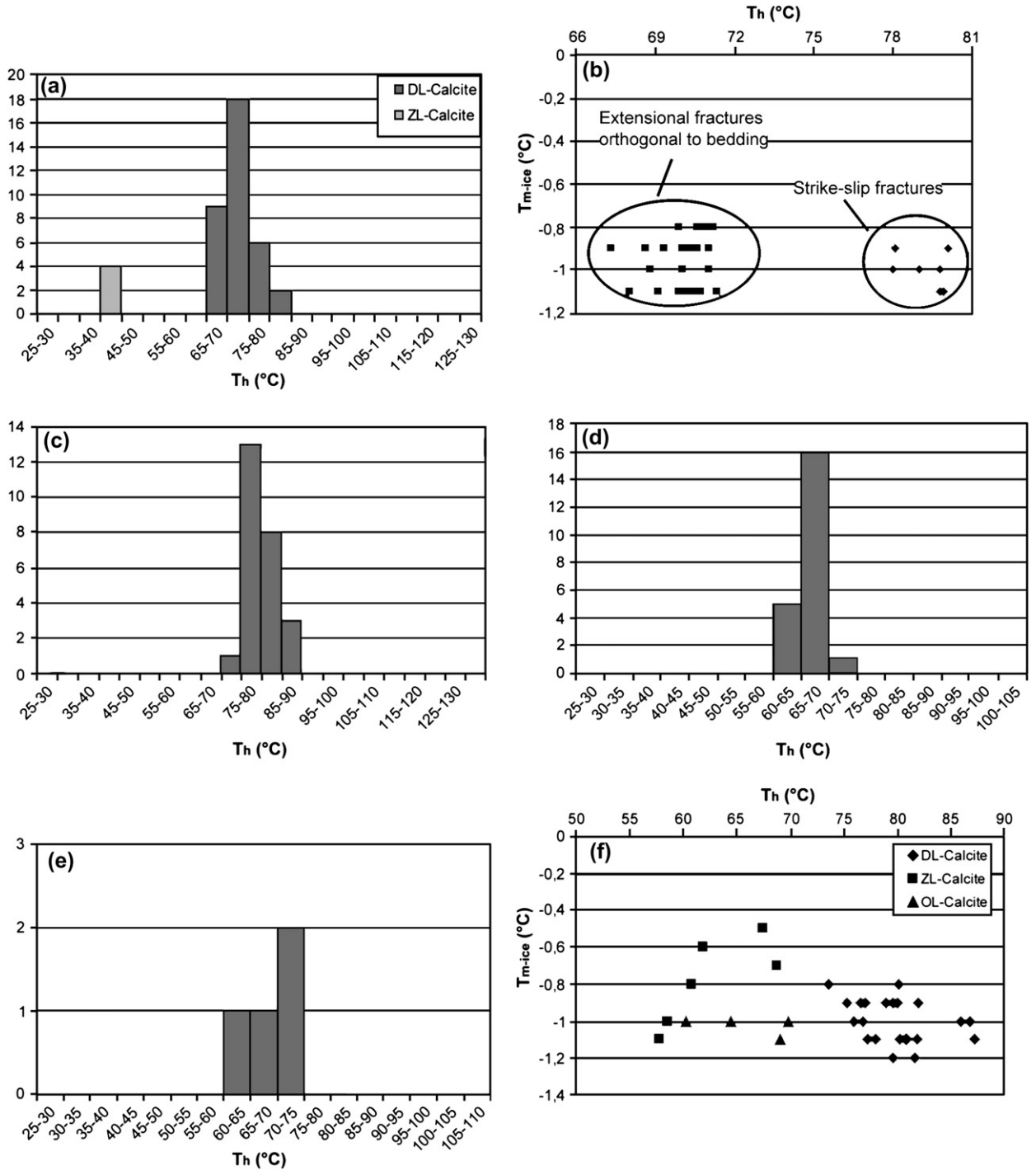

Fig. 11. Fluid inclusion microthermometric data from the Cava Filippi outcrop: (a) T_h histogram of primary inclusions in DL-calcite (dark grey) and of sporadic primary inclusions in ZL-calcite (light grey); (b) $T_h/T_{m\text{-}ice}$ diagram for primary fluid inclusions in DL-calcite: data from strike-slip fractures show slightly higher value of T_h (about 10 °C). Fluid inclusion data from Cemetery outcrop; (c) T_h histogram of primary fluid inclusions in DL-calcite; (d) in ZL-calcite; (e) in OL-calcite; (f) fluid inclusions $T_h/T_{m\text{-}ice}$ diagram.

mono-phase (all-liquid) fluid inclusions and not completely healed inclusion planes prevail. This kind of shape is generally typical of low entrapment temperatures (Roedder, 1984; Goldstein and Reynolds, 1994). This interpretation is here confirmed by a few T_h data from sporadic two-phase inclusions (T_h values < 50 °C; Fig. 11a) measured in ZL-calcite. $T_{m\text{-}ice}$ data from ZL- and OL-calcite, range between -1 °C and -0.8 °C and correspond to low salinity water (Bodnar, 1993).

In the Cemetery outcrop (Fig. 11f), $T_{m\text{-}ice}$ confirms the same values of the previous outcrop, allowing us to hypothesize a homogeneous fluid system, whereas T_h always has a slightly higher value (mean values of 79.6 °C in DL-calcite, 61.2 °C in ZL-calcite, and 64.5 °C in OL-calcite; Fig. 11c–e).

Table 2
Data from fluid inclusion analyses sorted by type of structure and calcite cement

Structures	Calcite type	Fluid inclusion T_h (°C)	
		Cava Filippi outcrop	Cemetery outcrop
Strike-slip fractures	DL	79	–
Extensional fractures orthogonal to bedding	DL	70	80
Open-extensional/shear fractures	ZL/OL	<50	61
Synthetic or antithetic low-angle slip planes	DL	–	–
Random fabric cataclasite	ZL	<50	64.5
Hydraulic breccia	DL	–	–
Foliated cataclasites	OL	<50	64.5

Although the fluid inclusion data set is small, consistently higher (by ca. 10 °C) homogenization temperatures are preserved. This could indicate a relative deeper deformation occurring at the Cemetery site and seems to be consistent with the fact that deformation in the Cemetery outcrop involves lower stratigraphic levels. Table 2 shows data from fluid inclusion analyses by type of calcite cement and deformation structure.

$\delta^{18}O$ and $\delta^{13}C$ isotope analysis allows us to characterize the isotopic signature of fault-related calcites and the origin (meteoric, marine, hydrothermal, etc.) of the fluids from which those calcite phases precipitated (e.g. Travé et al., 1998; Boles and Grivetti, 2000; Pili et al., 2002). Twenty-three samples were analyzed (Table 1). Samples include all calcite cement types and the hosting limestone rock.

A $\delta^{18}O$ versus $\delta^{13}C$ graph is shown in Fig. 12. The $\delta^{18}O$ values of the host rock (HR) range from −4.8 to −2.6‰ PDB. DL-calcite shows similar values (from −4.13 to −2.2‰ PDB). ZL-calcite shows values ranging from −17.17 to −12.21‰ PDB, and OL-calcite from −17.9 to −11‰ PDB. The $\delta^{13}C$ values of the host rock (HR) range between 1.36 and 2.45‰ PDB, as well as those relative to DL-calcite (from 1.8 to 2.33‰ PDB). ZL-calcite ranges between 2 and 2.63‰ PDB, and OL-calcite $\delta^{13}C$ values range between 0.58 and 1.5‰ PDB.

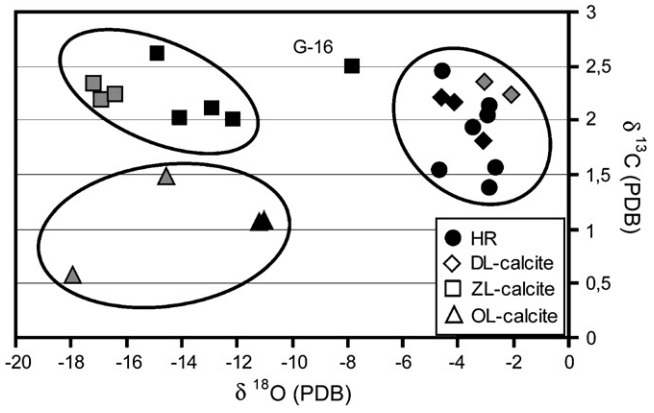

Fig. 12. Data from stable isotope analyses plotted in a $\delta^{18}O/\delta^{13}C$ graph: black samples are from the Cava Filippi outcrop and grey ones from the Cemetery outcrop (HR = host rock). For both outcrops three different poles can be depicted (circles). The G-16 anomalous samples probably included a small piece of the HR during powder preparation for analysis.

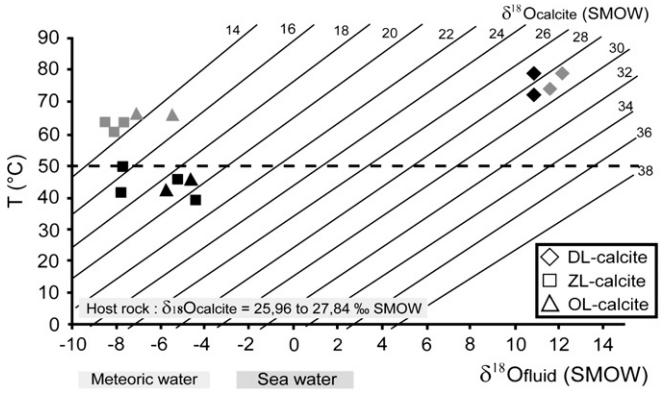

Fig. 13. Plot of values of $\delta^{18}O$-calcite in SMOW versus values of $\delta^{18}O$-fluid in SMOW with correction of the temperature, $T = f$ ($\delta^{18}O$-fluid): in black samples from the Cava Filippi outcrop and grey ones from the Cemetery outcrop. By modifying the temperature of crystallization, points move along the oblique lines of $\delta^{18}O$-calcite SMOW. In the abscissa, meteoric and sea water domain windows are indicated (applied from Benedicto et al., in press).

Data from both outcrops define three different grouping (Fig. 12): the first is formed by the host rock and DL-calcite which have very similar values of both $\delta^{18}O$ and $\delta^{13}C$, the second and the third are formed by the ZL-calcite and OL-calcite. ZL-calcite displays similar values of $\delta^{13}C$ to the HR pole, but different values of $\delta^{18}O$, while OL-calcite shows similar $\delta^{18}O$ values but slightly lower $\delta^{13}C$ values than the HR and the ZL pole. This indicates that the DL-calcite precipitated from a fluid in equilibrium with the HR for both stable isotopes, while ZL-calcite precipitated from a fluid equilibrated with the HR for the $\delta^{13}C$ but not for the $\delta^{18}O$ and OL-calcite precipitated from a fluid non-equilibrated with the HR for $\delta^{13}C$ or for the $\delta^{18}O$. This is consistent with the cathodoluminescence result. The G-16 anomalous probably included a small piece of the boundary HR during sample preparation for analysis.

In order to establish the fluid origin of calcite cements the O isotope composition is interpreted by using the crystallization temperatures estimated from fluid inclusion and the isotopic fractioning coefficients of Kim and O'Neil (1997). This is represented in Fig. 13 by the plot of $\delta^{18}O$ of calcite (values in SMOW, Standard Mean Ocean Water) versus $\delta^{18}O$ of fluid (SMOW) as a function of the temperature fields ($T = f$ ($\delta^{18}O_{fluid}$)). In the plot of Fig. 13 the horizontal axis indicates the domains of calcite origin from meteoric or marine water. By modifying the temperature of crystallization (fluid inclusion trapping temperatures), points move along the oblique $\delta^{18}O$-calcite SMOW lines. Our results allowed us to evaluate two fluids which precipitated the three types of calcite cements: one fluid is rich in $\delta^{18}O$ (DL-calcite) and the other is poor in $\delta^{18}O$ (ZL- and OL-calcites). This suggests that the ZL- and OL-calcites formed from meteoric water (poor in $\delta^{18}O$) at a maximum temperature of 65 °C in the Cemetery

Table 3
Data from ICP-AES analyses showing Fe, Mn, Mg, Sr, and Si ion percentage in the analyzed samples

Samples	Calcite type	Fe (ppm)	Si (ppm)	Mn (ppm)	Mg (ppm)	Sr (ppm)
G-3	DL	1.94	0	0.55	1.95	0.99
G-13	ZL	0.61	0	0.35	1.5	0.39
G-29	OL	1.44	0	0.95	0.99	0.99
Gc-3	DL	1.08	0	0.71	1.1	0.71
Gc-13	ZL	0.82	0	0.55	0.62	1.74
Gc-12	OL	2.53	3.72	0.59	1.99	0.91

Cu, Zn, Al, Ni, and Pb ions were not detected in the analyzed calcites.

site and less than 50 °C in the Cava Filippi site. This water was in isotopic disequilibrium with the HR. The origin of fluid for the DL-cement is more delicate to interpret. DL-calcite formed from a fluid isotopically equilibrated with the host limestone. The $\delta^{18}O$ values of the DL-calcite are higher with respect to those reported for the Cretaceous rocks from marine origin (Pirrie and Marshall, 1990); this suggests a diagenetic alteration of the carbonates at shallow meteoric and/or burial conditions (Travé et al., 1998). Nevertheless, DL-calcite shows $\delta^{18}O$-fluid SMOW values higher than observed for meteoric water and sea water. In fact, they are higher than highest values observed for marine basin brines (Kharaka and Carothers, 1986).

ICP-AES analyses were performed in order to help the interpretation of fluid origin. For both outcrops one sample for each type of calcite was analyzed. Fe, Mn, Mg, Sr, Si, Cu, Zn, Al, Ni, and Pb ion composition percentage (ppm; Table 3) was investigated. Cu, Zn, Al, Ni, and Pb ions are under the detected limit of the ICP-AES. Fe, Mn, Mg, and Sr ion concentrations do not show significant differences in any all type of calcites. This suggests that all calcites have overall the same composition and that, based on the well-established origin of the ZL- and OL-calcites from stable isotope results, they all probably precipitated from meteoric water. Probably fluid having generated DL-calcite was involved in a longer diagenesis than fluids having generated ZL- and OL-calcite, but their origin could have been the same. Furthermore, the same fluid origin is also suggested by fluid composition with very low salinity water measured from fluid inclusion analyses in all the different calcite types.

6. Fault displacement and deformation

It has often been suggested that the thickness of fault zones and gouges increases progressively as the fault displacement increases (e.g. Fossen and Hesthammer, 2000; Shipton and Cowie, 2001, 2003; Scholz, 1990). Recent work shows that in faults involving porous carbonate rocks, fault gouge thickness increases with the displacement until a maximum value, after which the thickness of the gouge stabilises (Micarelli et al., 2006). Here we investigate the relationship between normal fault displacement and the deformation structures observed through the Gubbio fault zone, mainly involving non-porous carbonate rocks.

In the present work, some stratigraphic controls on the sequence involved within the fault zone have been carried out in order to evaluate fault displacement. This is represented in Fig. 14 where the stratigraphic column (Fig. 14a; Premoli Silva and Sliter, 1994), the location of the studied samples, in both outcrops (Fig. 14b, c), and the displacement calculation (Fig. 14d) are shown. Error bars in the micropaleontological data are important and introduce scatter in the estimation of fault displacements.

In the Cava Filippi outcrop, the estimated displacement between Df-0 and Df-1, i.e. for Ff-1, is negligible (3 ± 27 m). This is consistent with: (i) the small amount of deformation observed within the Df-1. Layers are tilted, only slightly perturbed by open main extensional fractures; and (ii) the absence of random fabric cataclasite associated to Ff-1. Only hydraulic breccia is associated with this fault. Relative displacement between Df-1 and Df-2 is 130 ± 30 m therefore ranging between 100 and 160 m. Random fabric cataclasite characterizes the Ff-2 fault plane. Within the Df-2, analyzed samples indicate an intra-domain displacement between the lower and the upper parts of 25 ± 25 m, ranging from 0 to 50 m maximum. This is accommodated by well-developed sigmoidal shear planes and extensional duplex structures. Although the presence of foliated cataclasites constitutes the Df-3 domain, displacement between domains Df-2 and Df-4 cannot be >50 m. In contrast, displacement can increase up to around 90 m (60 ± 30 m) when moving toward Df-5. Foliated cataclasites of Df-3 domain seem to be related to a lithological change (from well-bedded limestones to more clay rich red limestones) rather than to a large amount of displacement. Cumulative displacement within this outcrop ranges between a minimum of 150 m and a maximum of 230 m.

A similar order of magnitude of displacement is calculated in the Cemetery outcrop. Relative displacement between Dc-0 and Dc-1 is around 138 ± 82 m. Dc-1 and Fc-1 are characterized by associated foliated cataclasites. Here, a combined influence of both displacement and lithology (from the *Marne a Fucoidi Fm* to the *Scaglia rossa Fm*) on foliated cataclasites development cannot be neglected. While displacement between Dc-1 and Dc-2 is negligible, the displacement between Dc-2 and Dc-3 is 158 ± 47 m, ranging between 110 and 205 m and displacement between Dc-3 and Dc-4 can reach 40–45 m. In this outcrop, cumulated displacement ranges between 300 and 375 m.

Therefore, all the observed deformation and related structures of the studied fault zone result from not more than 230 m of vertical displacement for the Cava Filippi outcrop and not more than 375 m for the Cemetery outcrop, which represent, respectively, only the 12–19% of the total estimated geological throw for the Gubbio fault (Mirabella et al., 2004). This percentage of displacement involves a 50 m thick zone in which an original stratigraphic sequence of about 230–380 m has been sheared, indicating a very strong thinning of the fault-involved limestones corresponding to

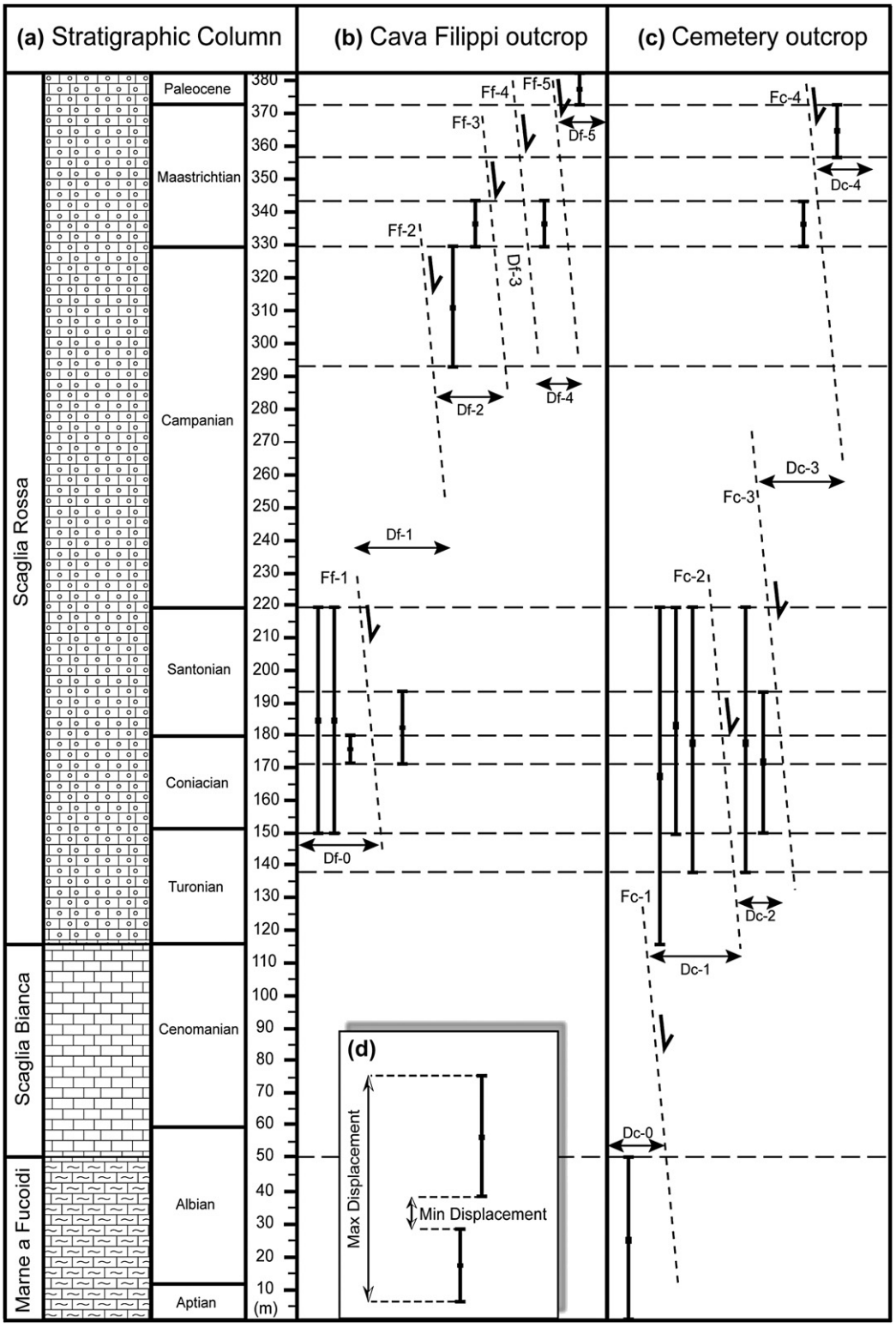

Fig. 14. Fault displacement evaluation from biostratigraphic controls: (a) whole stratigraphic column reconstructed from the Bottaccione section by Premoli Silva and Sliter (1994); (b) the Cava Filippi outcrop samples location; (c) the Cemetery outcrop samples location; (d) schematic diagram showing how displacement is calculated.

70–85% of the initial thickness. Thinning can be explained by stretching due to extensional and shear structures but, probably, dissolution processes can also play an important role. In fact, if we consider the minimum value of displacement due to mechanical stretching, the contribution of dissolution to the thinning of the stratigraphic sequence may be estimated up to a maximum of 35% in the Cava Filippi outcrop and up to a maximum of 20% in the Cemetery outcrop.

7. Interpretation of fault evolution

The fault zone in the two outcrops along the Gubbio fault is around 50 m thick and is characterized by several structural domains separated by well-defined main slip planes. Calculated displacements suggest relatively small throw accommodated through the observed fault zone (230–375 m) which only represents 12–19% of the total fault throw attributed to the Gubbio fault by Mirabella et al. (2004) and the largest throw is therefore inferred to occur along the major fault escarpment which bounds the outcrops to the west (Figs. 3 and 4).

Different types of tectonic structures and fault rocks developed within the fault zone. Most of the tectonic structures are partially or completely filled by synfaulting calcite. Three types of calcite cements are recognized (DL-, ZL-, and OL-types). Cross-cutting relationships indicate that structures filled by the DL-cement (strike-slip and orthogonal to bedding fractures, secondary low-angle slip planes in both outcrops and the hydraulic breccia in the Cava Filippi outcrop) formed first. Paleothermometry data indicate that strike-slip and orthogonal to bedding fractures formed at temperatures around 70–80 °C, i.e. at depth of around 2500–2800 m, taking into account a normal paleogeothermal gradient of 30 °C/km. The fact that strike-slip and orthogonal to bedding fractures are present also outside the fault zone, and the orthogonal to bedding fractures are always tilted together with the bedding and they are found reworked in the outer domains indicating that these types of structures preceded the main extensional phase as already suggested by De Paola et al. (2006). Kinematic data from the conjugate strike-slip fractures are consistent with a NW–SE compression and a NE–SW oriented extension.

Cathodoluminescence and isotope analyses indicate that the hydraulic breccia and the secondary low-angle planes were cemented by calcite precipitated from the same fluid and in a closed system (i.e. confined at depth) like the strike-slip and orthogonal to bedding fractures calcite filling. Hydraulic breccia and secondary low-angle planes in Df-0 of the Cava Filippi outcrop recorded the first stages of extensional faulting at depth.

ZL- and OL-calcites that cemented and filled open-extensional/shear fractures, random cataclasite associated to major slip planes, foliated cataclasites, shear zones and the hydraulic breccia in the Cemetery outcrop, precipitated at temperatures lower than 60–65 °C, and have very similar isotopic compositions. The differences in $\delta^{18}O$ (Fig. 12) are very small to seem significant. This indicates the same water origin for both calcite types. These tectonic structures probably formed later at depths shallower than 2000 m, suggesting that extensional faulting occurred in a context of progressive exhumation of the footwall block.[5] Nevertheless, deformation must have occurred at all times at sufficient depth to be out of the influence of the surface flooding water, as indicated by the geochemical analysis that shows that ZL- and OL-calcites were equilibrated in $\delta^{13}C$ with the host rock limestone (when in meteoric water it is expected a constant disequilibrium in both the $\delta^{18}O$ and the $\delta^{13}C$ between the water and the host rock). Although the ZL- and OL-calcites display high values of $\delta^{18}O$ than DL-calcite, the ICP-AES and the salinity of fluid inclusions suggest the same meteoric origin for all of them. Most probably, DL-calcite simply formed deeper from a fluid that resided long enough time within the host rock to be equilibrated both in $\delta^{18}O$ and $\delta^{13}C$ while ZL- and OL-calcites probably formed from meteoric water that resided long enough to be equilibrated in $\delta^{13}C$ but not enough to be equilibrated in $\delta^{18}O$. Although ZL- and OL-calcites probably have the same water origin, in the Cava Filippi outcrop, they fill structures that are located in different structural domains and never mix into the same structure. The ZL-calcite appears in the Df-0 and in the lower part of the Df-2, below Ff-6, while the OL-calcite appears from the Df-2, above Ff-6, through the Df-5 (Fig. 3). ZL-calcite completely cements the random cataclasites associated to the main slip fault planes, and completely or partially fills the open-extensional/shear fractures. When these fractures were partially filled, the calcite is of the drusy type. Open-extensional/shear fractures seem to accommodate rotation and shear of Df-1 and Df-2 domains during major slip plane activity and random cataclasites development. The fact that open-extensional/shear fractures are sometimes partially filled while the cataclasites completely cemented can suggest either a very rapid opening of fractures or that the fluid moved preferentially toward the zone of cataclasis. Hydraulic breccia was reactivated during this tectonic phase, as suggested by the ZL-calcite filling partially empty voids within the DL-cement.

OL-calcite is located in the foliated cataclasites and in the shear zones in the most basinwards domains, where ZL-calcite is absent, and the DL-calcite appears as reworked pieces. The limit between ZL- and OL-calcites is defined by the Ff-6 fault, which is sub-parallel to the bedding in this structural domain and oblique to Ff-2 and Ff-3 (Fig. 3). This fault, at the outcrop scale, represents a simple shear plane underlain by a thin rim of gouge which seems an insufficient feature to constitute a fluid circulation barrier. However, differences in water composition can be related to lithological changes. Rocks of different porosity can constitute different disconnected aquifers. At this point of knowledge, two scenarios are possible: different water circulating separately in each lithology during synchronous deformation in the whole damage zone; or, as the marly stratigraphic sequence of the inner domains is younger in age, foliated cataclasites and shear zones of the inner domains formed later than the structures filled by the ZL-calcite, at shallower depth, i.e. in a shallower aquifer, during the upward propagation of the fault through the stratigraphic sequence.

The extensional deformation process of the Gubbio fault started with hydraulic brecciation (Ff-1) and low-angle faulting in the inner domain (Df-0). The faulting process, probably related to the upward fault tip propagation, evolved while synchronous footwall exhumation occurred. Successively, deformation progressively localized in narrower zones, where slip planes and cataclastic processes developed. Shear and rotation of structural domains between the slip planes induced

[5] In fact, the fault zone in the two outcrops ≪sticks≫ to the footwall block and the damage zone is observed to pass laterally to undeformed footwall carbonate.

open-extensional/shear fracturing in the more brittle grey/white limestones and the development of foliated cataclasites in the more ductile marly limestones. Deformation progressively moved basinwards through a large fault zone. This occurred at a depth where relatively old meteoric water was separated from the influence of the surface flooding water. Based on our interpretation, stylolites developed during the entire deformation process. Finally, as the fault propagated upwards, exhumation progressed, and deformation occurred closer or at the surface, localized on the major topographic fault escarpment which separates the basin from the footwall and that probably has accommodated about 80–90% of geological throw. Therefore, fault zones analyzed in the two studied outcrops developed in the early stages of the development of the Gubbio fault, preceding major displacement accumulations (which occurred along the major scarp to the west).

8. Concluding remarks

Our work highlights several interesting aspects relative to deformation along the Gubbio fault which can be summarized as follows:

(i) The structural style of the Gubbio fault zone is characterized by a damage zone intensely deformed and rich in deformation structures (open-extensional/shear fractures, shear planes, duplex structures, several main highly-dipping and secondary low-angle slip planes, shear zones dissolution seams) and related fault rocks (hydraulic breccia, random and foliated cataclasites).
(ii) This structural style attests to deformation occurring while confined at a relative depth and for a progressive exhumation of the fault zone, but it contrasts with the relatively small amount of fault displacement accommodated by this section of the entire fault zone (only the 12–19% of the cumulated total displacement).
(iii) This percentage of displacement involves a 50 m thick zone in which an original stratigraphic sequence of about 230–380 m has been sheared. This indicates a very strong thinning of the fault-involved limestones corresponding to 70–85% of the initial thickness.
(iv) Some of the deformation processes that should be expected to be related to the amount of displacement (as random and foliated cataclasites) do not here have a clear relationship with the displacement magnitude and lithology seems to play an important role instead.
(v) Stretching due to extensional and shear structures and dissolution processes were also important.

Acknowledgments

We thank Marina Gillon and Elena Crespi for help on isotopes analyses, Petros Didaskalou for stratigraphic controls and Laura Petetta for the help on ICP-AES analyses. We also thank Jean-Pierre Villotte, Aldo Marchionni and Valérie Godard for the preparation of thin/thick and polished sections. We thank J.P. Craddock and S. Mazzoli for their detailed reviews and constructive comments that helped to improve the manuscript. We also thank R. Schultz for a complementary and critical reading. This work was funded by a ''Foreign Improvement Grant'' (University of Camerino) and FAR Invernizzi 2005 Project with research facilities from the Laboratoire de Tectonique UMR 7072 of the French CNRS.

References

Alfano, A., Decandia, F.A., Lavecchia, G., Pialli, G.P., Biella, G., Lozej, A., Treves, B., 1982. Profilo Piombino-Ancona: dati geofisici ed interpretazione geologica. Bollettino della Società Geologica Italiana 101, 247–258.

Barchi, M.R., Minelli, G., Pialli, G., 1998. The CROP 03 profile: a synthesis of results on deep structures of the northern Apennines. Memorie della Società Geologica Italiana 52, 383–400.

Barchi, M., Paolacci, S., Pauselli, C., Pialli, G., Merlini, S., 1999. Geometria delle deformazioni estensionali recenti nel bacino dell'Alta Val Tiberina fra S.Giustino Umbro e Perugina: evidenze geofisiche e considerazioni geologiche. Bollettino della Società Geologica Italiana 118, 617–625.

Barchi, M.R., Galadini, F., Lavecchia, G., Messina, P., Michetti, A.M., Peruzza, L., Pizzi, A., Tondi, E., Vittori, E., 2000. Sintesi sulle conoscenze delle faglie attive in Italia Centrale. Gruppo Nazionale per la Difesa dei Terremoti.

Benedicto, A., Plagnes, V., Vergely, P., Flotté, N., Schultz, R.A. Fault and fluid interaction in a rifted margin: integrated study of calcite-sealed fault-related structures (southern Corinth margin). In: Wibberley, C.A.J., Kurtz, W., Imber, J., Holdsworth, R.E., Collettini, C. (Eds.). The Internal Structure of Fault Zones: Implications for Mechanical and Fluid-Flow Properties. Geological Society, London, Special Publications, in press.

Bodnar, J.R., 1993. Revised equation and table for determining the freezing point depression of H_2O–NaCl solution. Geochimica et Cosmochimica Acta 57, 683–684.

Boles, J.R., Grivetti, M., 2000. Calcite cementation along the Refugio/Carneros fault, coastal California: a link between deformation, fluid movement and fluid–rock interaction at a basin margin. Journal of Geochemical Exploration 69–70, 313–316.

Boncio, P., Ponziani, F., Brozzetti, F., Barchi, M., Lavecchia, G., Pialli, G., 1998. Seismicity and extensional tectonics in the northern Umbria–Marche Apennines. Memorie della Società Geoleologica Italiana 52, 539–555.

Boncio, P., Brozzetti, F., Lavecchia, G., 2000. Architecture and seismotectonics of a regional low-angle normal fault zone in Central Italy. Tectonics 19, 1038–1055.

Boncio, P., Lavecchia, G., 2000. A structural model for active extension in Central Italy. Journal of Geodynamics 29, 233–244.

Boschi, E., Guidoboni, E., Ferrari, G., Valensise, G., Gasperini, P., 1997. CFTI, Catalogo dei Forti Terremoti Italiani dal 461 a.C. al 1990. Istituto Nazionale di Geofisica, Storia Geofisica Ambientale, Bologna.

Calamita, F., Pizzi, A., 1994. Recent and active extensional tectonics in the southern Umbro-Marchean Apennines (Central Italy). Memorie della Società Geologica Italiana 48, 541–548.

Cello, G., Mazzoli, S., Tondi, E., Turco, E., 1997. Active tectonics in the central Apennines and possible implications for seismic hazard analysis in peninsular Italy. Tectonophysics 272, 43–68.

Cello, G., Invernizzi, C., Mazzoli, S., Tondi, E., 2001. Fault properties and fluid flow patterns from quaternary faults in the Apennines, Italy. Tectonophysics 336, 63–78.

Collettini, C., Barchi, M., Pauselli, C., Federico, C., Pialli, C., 2000. Seismic expression of active extensional faults in northern Umbria (Central Italy). Journal of Geodynamics 29, 309–321.

Collettini, C., Barchi, M.R., 2002. A low-angle normal fault in the Umbria region (Central Italy): a mechanical model for the related microseismicity. Tectonophysics 359, 97–115.

Collettini, C., Barchi, M.R., Chiaraluce, L., Mirabella, F., Pucci, S., 2003. The Gubbio fault: can different methods give a picture of the same object? Journal of Geodynamics 36, 51–66.

Craig, H., 1957. Isotope standards for carbon and oxygen and correction factors for mass-spectrometric analysis of carbon dioxide. Geochimica et Cosmochimica Acta 12, 133–149.

Deiana, G., Pialli, G., 1994. The structural provinces of the Umbro-Marchean Apennines. Memorie della Società Geologica Italiana 48, 473–484.

De Paola, N., Mirabella, F., Barchi, M.R., Burchielli, F., 2006. Early orogenic normal faults and their reactivation during thrust belt evolution: the Gubbio fault case study, Umbria–Marche Apennines (Italy). Journal of Structural Geology 28, 1948–1957.

Dewey, J.F., Helman, M.L., Turco, E., Hutton, D.H.W., Knott, S.D., 1989. Kinematics of the western Mediterranean. In: Coward, M.P., Dietrich, D., Park, R.G. (Eds.), Alpine Tectonics. Geological Society, London, Special Publication, vol. 45, pp. 265–283.

Elter, P., Giglia, G., Tongiorgi, M., Trevisan, L., 1975. Tensional and compressional areas in the recent (Tortonian to present) evolution of the northern Apennines. Bollettino di Geofisica Teorica ed Applicata 17, 3–19.

Fossen, H., Hesthammer, J., 2000. Possible absence of small faults in the Gullfaks Field, northern North Sea: implication for downscaling of faults in some porous sandstones. Journal of Structural Geology 22, 851–863.

Goldstein, R.H., Reynolds, T.J., 1994. Systematics of Fluid Inclusions in Diagenetic Minerals. In: SEMP Short Course, no. 31. USA.

Harding, T.P., Tuminas, A.C., 1989. Structural interpretation of hydrocarbon traps sealed by basement normal faults at stable of foredeep basins and at rift basins. AAPG Bulletin 73, 812–840.

Kastens, K., Mascle, J., Auroux, C., Bonatti, E., Broglia, C., Channell, J.E.T., Curzi, P., Kay-Cristian, E., Glacon, G., Hasegawa, S., Hieke, W., McCoy, F., McKenzie, J., Mendelson, J., Muller, C., Rehault, J.P., Robertson, A., Sartori, R., Sprovieri, R., Torii, M., 1988. ODP leg 107 in the Tyrrhenian Sea: insights into passive margin and back-arc basin evolution. Geological Society of America Bulletin 100, 1140–1156.

Kharaka, Y.K., Carothers, W.W., 1986. Oxygen and hydrogen isotope geochemistry of deep basin brines. In: Fritz, P., Fontes, J.Ch. (Eds.), Handbook of Environmental Isotopes Geochemistry: The Terrestrial Environment, vol. 2. Elsevier, pp. 305–360.

Kim, S.T., O'Neil, J.R., 1997. Equilibrium and non-equilibrium oxygen isotope effects in synthetic carbonates. Geochimica et Cosmochimica Acta 61, 3461–3475.

Labaume, P., Carrio-Schaffhauser, E., Gamond, J.F., Renard, F., 2004. Deformation mechanisms and fluid-driven mass transfers in the recent fault zones of the Corinth rift (Greece). Comptes Rendus Geoscience 336, 375–383.

Lindsay, N.G., Murphy, F.C., Walsh, J.J., Watterson, J., 1993. Outcrop studies of shale smear on fault surfaces. In: International Association of Sedimentologist, Special Publication, vol. 15, pp. 113–123.

Maltman, A.J., 1998. Deformation structures from the toes of active accretionary prism. Journal of the Geological Society (London) 155, 639–650.

Menichetti, M., Minelli, G., 1991. Extensional tectonics and seismogenesis in Umbria (Central Italy): the Gubbio area. Bollettino della Società Geologica Italiana 110, 857–880.

Micarelli, L., Benedicto, A., Invernizzi, C., Saint-Bezar, B., Michelot, J.L., Vergely, P., 2005. Influence of *P/T* conditions on the style of normal fault initiation and growth in limestones from the SE-Basin, France. Journal of Structural Geology 27 (9), 1577–1598.

Micarelli, L., Benedicto, A., Wibberley, C.A.J., 2006. Structural evolution and permeability of normal fault zones in highly porous carbonate rocks. Journal of Structural Geology 28 (7), 1214–1227.

Mirabella, F., Ciaccio, M.G., Barchi, M.R., Merlini, S., 2004. The Gubbio normal fault (Central Italy): geometry, displacement distribution and tectonic evolution. Journal of Structural Geology 26, 2233–2249.

Munchez, P., Marshall, J.D., Touret, J.L.R., Viaene, W.A., 1994. Origin and migration of paleofluids in the Upper Visean of Campine Basin, northern Belgium. Sedimentology 41, 133–145.

Pauselli, C., Federico, C., 2003. Elastic modeling of the Alto Tiberina normal fault (Central Italy): geometry and lithological stratification influences on the local stress field. Tectonophysics 374, 99–113.

Pili, E., Poitrasson, F., Gratier, J.P., 2002. Carbon–oxygen isotope and trace element constraints on how fluids percolate faulted limestones from the San Andreas Fault system: partitioning of fluid sources and pathways. Chemical Geology 190, 231–250.

Pirrie, D., Marshall, J.W., 1990. High-paleolatitude late cretaceous paleotemperature: new data from James Ross Island, Antarctica. Geology 18, 31–34.

Premoli Silva, I., Sliter, W.V., 1994. Cretaceous planktonic foraminiferal biostratigraphy and evolutionary trends from the Bottaccione section, Gubbio, Italy. Palaeontographia Italica 82, 1–89 (Pisa 1994 (Stratigrafia Cretacico It. n.5)).

Roedder, E., 1984. Fluid inclusions. In: Reviews in Mineralogy, vol. 12.

Scholz, C.H., 1990. The Mechanism of Earthquakes and Faulting. Cambridge University Press.

Shipton, Z.K., Cowie, P.A., 2001. Damage zone and slip-surface evolution over μm to km scales in high-porosity Navajo sandstone, Utah. Journal of Structural Geology 23, 1825–1844.

Shipton, Z.K., Cowie, P.A., 2003. A conceptual model for the origin of fault damage zone structures in high-porosity sandstone. Journal of Structural Geology 25, 333–344.

Sibson, R.H., 2000. Fluid involvement in normal faulting. Journal of Geodynamics 29, 469–499.

Travé, A., Calvet, F., Soler, A., Labaume, P., 1998. Fracturing and fluid migration during Paleogene compression and Neogene extension in the Catalan Coastal Range, Spain. Sedimentology 45, 1063–1082.

Vityk, M.O., Bodnar, R.J., 1995. Textural evolution of synthetic fluid inclusions in quartz during reequilibration, with application to tectonic reconstruction. Contributions to Mineralogy and Petrology 121 (3), 309–323.

Weber, K.J., Mandl, G., Pilaar, W.F., Lehner, F., Precious, R.G., 1978. The role of faults in hydrocarbon migration and trapping in Nigerian growth fault structures. In: Tenth Annual Offshore Technology Conference Proceedings.